

8-6-2007

The Hydrolysis of Naphthalene Diimides

Michelle B. Kim
Michelle.kim25@gmail.com

Follow this and additional works at: http://digitalarchive.gsu.edu/chemistry_theses

Recommended Citation

Kim, Michelle B., "The Hydrolysis of Naphthalene Diimides" (2007). *Chemistry Theses*. Paper 7.

This Thesis is brought to you for free and open access by the Department of Chemistry at Digital Archive @ GSU. It has been accepted for inclusion in Chemistry Theses by an authorized administrator of Digital Archive @ GSU. For more information, please contact digitalarchive@gsu.edu.

THE HYDROLYSIS OF NAPHTHALENE DIIMIDES

by

MICHELLE B. KIM

Under the Direction of Dabney W. Dixon

ABSTRACT

The hydrolyses of naphthalene diimides (NDIs) bearing aliphatic side chains with *N*-methylpyrrolidinium groups placed two (**1**) and three (**5**) atoms from the central core were studied. The K_a values for the first and second hydrolyses for **1** were $2.5 \pm 0.2 \times 10^5 \text{ M}^{-1}$ and $2.0 \pm 0.1 \times 10^2 \text{ M}^{-1}$, respectively; for **5** they were $1.4 \pm 0.1 \times 10^5 \text{ M}^{-1}$ and $44 \pm 2 \text{ M}^{-1}$, respectively. NDI **1** hydrolyzed 6.8 times faster than did **5**. The rates for the first and second hydrolyses of **1** at 100 mM hydroxide measured by stopped-flow were $17.0 \pm 0.2 \text{ s}^{-1}$ and $53.0 \pm 0.1 \times 10^{-2} \text{ s}^{-1}$, respectively. NMR showed both the *syn* and *anti* isomers of the diamide species. Syntheses of other derivatives are reported. Overall, this study shows that the rate of hydrolysis of NDIs is increased when the cationic charge is moved closer to the NDI core.

INDEX WORDS: Hydrolysis, naphthalene diimide, diimide, monoimide, diamide, borate buffer.

THE HYDROLYSIS OF NAPHTHALENE DIIMIDES

by

MICHELLE B. KIM

A Thesis Submitted in Partial Fulfillment of the Requirements for the Degree of

Master of Science

in the College of Arts and Sciences

Georgia State University

2007

Copyright by
MICHELLE B. KIM
2007

THE HYDROLYSIS OF NAPHTHALENE DIIMIDES

by

MICHELLE B. KIM

Major Professor: Dabney W. Dixon
Committee: Giovanni Gadda
Kathryn B. Grant

Electronic Version Approved:

Office of Graduate Studies
College of Arts and Sciences
Georgia State University
August 2007

ACKNOWLEDGEMENTS

I would first like to thank God for the opportunity to continue with my education.

I would like to thank my parents Julie and Jung-Hyun, my brother David, my fiancé Cin and all of my friends who have loved, supported, and encouraged me.

I would like to thank Dr. Dabney Dixon for lending me her strength and knowledge and for all her guidance and direction.

I would like to thank the members of my committee, Dr. Kathryn Grant and Dr. Giovanni Gadda for their support and cooperation

Last, but not least, I would like to thank all of the Dixon, Grant, and Gadda group, especially Brian Sook, Kyle Chan, Melissa Sprague, Giselle Delgado, and Brian Basden, for all the learning moments and good times that we shared in and out of the lab.

TABLE OF CONTENTS

ACKNOWLEDGEMENTS	iv
LIST OF TABLES	vii
LIST OF FIGURES	viii
CHAPTER 1	
1.1.1 INTRODUCTION	1
1.2 EXPERIMENTAL	
1.2.1 Materials	3
1.3 RESULTS	
1.3.1 Synthesis	7
1.3.2 UV-visible absorbance spectroscopy	8
1.3.3 NMR and capillary electrophoresis studies	9
1.3.4 Kinetics of ring hydrolysis: diimide to monoimide	10
1.3.5 Kinetics of ring hydrolysis: monoimide to diamide	10
1.4 DISCUSSION	
1.4.1 The kinetics and equilibria of ring opening	11
1.4.2 <i>Syn</i> and <i>anti</i> isomers of the diamide	13
CHAPTER 2	
2.0 Naphthalene diimides in chemistry	27
2.1 SYNTHESIS	
2.1.1 Preparation of naphthalene diimides	28
2.1.2 Diethyl Derivative	28
2.1.3 Alkylation	29

2.1.4 Monoalkylated diimides	30
2.2 LITERATURE STUDIES	
2.2.1 Hydrolysis of NDI	31
2.2.2 Kinetics of the hydrolysis of NDI	32
2.2.3 Diimide-lactam rearrangement	34
2.2.4 Hydrolysis of naphthalene tetracarboxylic dianhydride	35
2.2.5 Possible buffer contribution to hydrolysis	35
2.3 EXPERIMENTAL STUDIES	
2.3.1 Recording the spectrum of the monoimide	37
2.3.2 Determination of K_a	38
2.3.3 Attempted reclosing of the diimide	39
2.3.4 ^1H NMR spectroscopy	39
2.3.5 Stopped-flow kinetics	41
2.3.6 Calculating k_r	43
2.3.7 Buffer contribution	44
2.3.8 The position of the charge in the side chain affects the rate of hydrolysis	45
2.4.0 CONCLUSIONS	45

LIST OF TABLES

Table 2.1. Chemical shifts of the geometric isomers of the diamide form of 1 in D ₂ O at selected temperatures. Only the two inner peaks of the AB-quartet are reported for the <i>anti</i> isomer	47
Table 2.2. The k_f and k_r of NDIs 1 and 5 . UV-visible experiments were performed in borate buffer; the stopped-flow experiment was run without buffer. The k_f and the k_r are derived from the slopes and the intercepts, respectively, of the rates as a function of [OH ⁻]	47
Table 2.3. Average k_{obs} for both processes at each concentration of NaOH (calculated using serial dilutions) from stopped-flow data	48
Table 2.4. The theoretical and experimental concentrations of NaOH and the differences between them	48
Table 2.5. Calculated k_f using fractions of HA and A ⁻ from equilibrium data	49
Table 2.6. Using $k = 161 \text{ M}^{-1} \text{ s}^{-1}$ (from stopped-flow data) to find k_{calc} (see text)	49

LIST OF FIGURES

CHAPTER 1

1.1. NDI derivatives in this study.	15
1.2. UV-visible absorbance spectra of 1 as a function of time (50 mM borate buffer at pH 9.0 with scans taken every 10 min for 50 min).	16
1.3. Mechanism of base-catalyzed hydrolysis of naphthalene diimides.	17
1.4. UV-visible spectra of the diimide, monoimide, and diamide.	18
1.5. Fractions of the diimide, monoimide and diamide as a function of pH. Samples of 1 were equilibrated in a buffer containing 100 mM sodium phosphate and 100 mM sodium tetraborate.	19
1.6. ^1H NMR at 600 MHz of compound 1 in D_2O at pH 12. The inset is the set of peaks at 7.4 ppm which is the diamide species (see text).	20
1.7. Electropherogram of NDI 1 (15.0 min) and its monoimide (28.6 min) using 25 mM sodium tetraborate buffer, pH 9.0, 11 kV.	21
1.8. Rate constants as a function of the concentration of hydroxide for the first hydrolysis of NDI 1 . Reactions were run at 25 °C in 100 mM borate buffer.	22
1.9. Rate constants as a function of the concentration of hydroxide for the first hydrolysis of NDI 5 . Reactions were run at 25 °C in 100 mM borate buffer.	23
1.10. Stopped-flow trace of the absorbance of NDI 1 as a function of $\log(\text{time})$ in 100 mM NaOH. Data were taken at 372 nm.	24
1.11. Absorbance as a function of time for 1 in 100 mM borate buffer at pH 9.6. The theoretical fit lies over the experimental points. Data were taken at 380 nm.	25
1.12. Absorbance as a function of time for 5 in 100 mM borate buffer at pH 9.6. The theoretical fit lies over the experimental points. Data were taken at 380 nm.	26

CHAPTER 2

2.1. Proposed mechanism for the synthesis of the imide ring.	50
2.2. NMR spectrum of monoalkylated 4 in D ₂ O. The inset shows the structure with the aromatic protons labeled.	51
2.3. Electropherogram of 4 and its monoalkylated precursor, 50 mM sodium phosphate buffer, pH 3.0, 11 kV.	52
2.4. (Left) Side chains of aromatic NDIs discussed in the text. (Center) Structure of the isoimide investigated by Ernst and Schmir (see text). (Right) Proposed intermediate in which borate acts as an intramolecular catalyst.	53
2.5. Proposed mechanism for the hydrolysis of the imide ring with borate as a nucleophilic catalyst.	54
2.6. Proposed mechanism for the hydrolysis of the imide ring with borate as a general base.	55
2.7. Absorbance of the diimide to monoimide of 1 as a function of pH. The reaction was run in 50 mM sodium phosphate buffer by adding aliquots of 0.1 M NaOH.	56
2.8. Absorbance of the monoimide to diamide of 1 as a function of pH. The reaction was run in 50 mM sodium phosphate buffer by adding aliquots of 0.1 M NaOH.	57
2.9. UV-visible spectra following the attempted ring closure of 1 in 50 mM sodium phosphate buffer by addition of aliquots of 12 M HCl.	58
2.10. Fractions of the diimide, monoimide and diamide as a function of pH. Samples of 5 were equilibrated in a buffer containing 100 mM sodium phosphate and 100 mM sodium tetraborate.	59
2.11. (Top) Designation of the aromatic protons on the NDI in the hydrolysis products. (Middle) ¹ H 300 MHz NMR spectrum of 1 in D ₂ O with the addition of NaOD. (Bottom) ¹ H 600 MHz NMR spectrum of 1 in D ₂ O after five days.	60
2.12. Difference spectra of the UV-visible absorbances for the three species of 1 . Difference spectra of the UV-visible absorbances for the diimide-monoimide (maximum at 380 nm) and monoimide-diamide (broad peak from 340 nm to 370 nm). The lines intersect at 372 nm, where the changes in absorbance between the species are the same.	61

2.13. Absorbance as a function of time for 1 in the presence of different concentrations of NaOH.	62
2.14. (Top) Rate of the first hydrolysis of 1 as a function of $[\text{OH}^-]$ calculated via serial dilution. (Bottom) Rate of the first hydrolysis of 1 as a function of $[\text{OH}^-]$ measured experimentally after completion of the reaction at the output of the system.	63
2.15. (Top) Rate of the second hydrolysis of 1 as a function of $[\text{OH}^-]$ calculated via serial dilution. (Bottom) Rate of the second hydrolysis of 1 as a function of $[\text{OH}^-]$ measured experimentally after completion of the reaction at the output of the system.	64
2.16. ^1H NMR spectrum of 1 at 300 MHz in D_2O .	65
2.17. ^1H NMR spectrum of 2 at 300 MHz in D_2O .	66
2.18. ^1H NMR spectrum of 3 at 300 MHz in D_2O .	67
2.19. ^1H NMR spectrum of 4 at 300 MHz in D_2O .	68
2.20. ^1H NMR spectrum of 5 at 300 MHz in D_2O .	69
2.21. Electrospray (ESI) high resonance mass spectrum from positive ion mode of NDI 1 . The exact mass is 461.2171 m/z.	70
2.22. Infrared spectrum of 1 .	71

List of Abbreviations

CE	Capillary electrophoresis
DNA	Deoxyribonucleic acid
k_f	Forward rate constant
k_r	Reverse rate constant
K_a	Equilibrium constant
NDI	Naphthalene diimide
NMR	Nuclear magnetic resonance spectroscopy
RNA	Ribonucleic acid
UV-visible	Ultraviolet- visible spectroscopy

Chapter 1

1.1.1 INTRODUCTION

Water-soluble naphthalene diimides (NDIs) have found uses in a wide variety of applications. They are excellent electron acceptors in aqueous solutions;¹⁻³ the photophysics of these species has been well-studied in water.⁴⁻⁹ Photolysis of NDIs has been used to reduce heme proteins;¹⁰ photoactivation of hydroperoxy derivatives has been used to oxidize both proteins^{4,11,12} and DNA.¹³⁻¹⁵ Selected NDI derivatives are examples of molecules that undergo spontaneous organization in aqueous solution.¹⁶⁻¹⁸

The majority of studies of NDI in aqueous solution have involved binding to nucleic acids. NDI derivatives have been known for many years to intercalate in duplex DNA.¹⁹⁻²¹ Study of NDI binding to DNA is now extensive; leading references to studies in the last ten years include those of binding to bulged duplexes,²² triplexes,^{23,24} quadruplexes,²⁵⁻²⁷ hairpins,²³ and DNA-RNA heteroduplexes.²⁸ Molecules with the NDI moiety have been shown to thread into DNA, with the diimide groups intercalating and the side chains or conjugating moieties lying in the grooves.²⁹⁻³³ The NDIs can carry reactive groups to the DNA including metal centers^{34,35} and alkylating agents.³⁶ Naphthalene diimides have been used to conjugate other nucleic acid binding species, thus increasing their binding^{37,38} and have been employed to stabilize DNA hairpins.³⁹ Diimides intercalated into or covalently bound to DNA have been used extensively in studies of photoinduced charge separation and charge recombination processes; leading references are given.⁴⁰⁻⁴⁵ The facile reduction of NDI bound to DNA has allowed these species to be used in the electrochemical detection of DNA.⁴⁶⁻⁴⁸

In general, studies of NDI with nucleic acids involve cationic substituents on the NDI side chains to favor electrostatic interactions between these side chains and the phosphate groups of the nucleic acid. Side chains with a methylene group adjacent to the imide nitrogen are necessary to prevent a steric clash between the side chain of the NDI and the DNA. A cationic center no further than three atoms away from the central core prevents self-stacking in aqueous solution, which can complicate DNA binding measurements.⁴⁹

Recently, we have synthesized four new NDI derivatives (**1** – **4**) with the cationic center two atoms away from the central core (Figure 1.1). Although such types of structures appear to be stable in neutral aqueous solution,^{3,19,22,50,51} we find that they are quite sensitive to base. It has been known for some time that the diimide ring system can react with alkali.⁵²⁻⁵⁴ Attack of hydroxide opens first one of the imide rings, and then the other, to give a diacid, diamide structure. Under forcing conditions, reaction of the diimide with base can lead to loss of CO₂ and contraction of one of the rings.^{55,56}

Herein, we present a study of the base-catalyzed hydrolysis of NDI derivatives with the cationic center both two and three atoms away from the central core. The former is far more labile to base both kinetically and thermodynamically. Stopped-flow and UV-visible absorbance studies as well as NMR data establish that the two imide rings in aliphatic naphthalene diimides are hydrolyzed sequentially.

1.2 Experimental

1.2.1 Materials

Nuclear magnetic resonance (NMR) spectra were recorded on Varian Unity+ 300 MHz and 600 MHz spectrometers. NMR samples for the parent NDIs were prepared in 0.5 ml of CDCl_3 (Aldrich) in 5 mm NMR tubes. NMR samples for alkylated derivatives were prepared in 0.5 ml of D_2O (Aldrich) in 5 mm NMR tubes. Capillary electrophoresis (CE) was carried out on a Beckman PACE 5500 instrument on a fused-silica capillary (60 cm x 75 μm i.d.) with a P/ACE diode array detector. The voltage used for electrophoresis was 11 kV and the sample was injected into the capillary using high pressure injection for 6 s. Reverse polarity was used where the sample was injected from the cathode and eluted to the anode. A mixture of NDI **4** and its monoalkylated precursor was injected in deionized water; the running buffer was 50 mM sodium phosphate at pH 3.0. A mixture of NDI **1** and its monoimide was injected in 50 mM sodium tetraborate buffer at pH 9.0; the running buffer was 50 mM sodium phosphate at pH 3.0. UV-visible spectra were recorded on a Varian Cary 50 UV-visible absorbance spectrophotometer. The mass spectra were taken on a Micromass Q-TOF spectrometer.

To determine the equilibrium constants, samples of **1** and **5** were equilibrated in buffer containing 100 mM sodium phosphate and 100 mM sodium tetraborate at approximately 10 pH values. Fractions of each of the diimide, monoimide and diamide were determined by taking linear combinations of the spectra of these three species. The fraction of the monoimide as a function of the concentration of hydroxide was fit to the equations in Chapter 2 using a nonlinear least squares fitting algorithm (Kaleidagraph, version 4.01, Synergy Software, Reading, PA) to determine K_{a1} and K_{a2} .

A HiTech Scientific SF-61 DX2 Double Mixing Stopped-Flow system equipped with temperature control was used to measure the absorption as a function of time after mixing at various pH values and to fit the stopped-flow kinetic data. The temperature was equilibrated to 25 °C. A xenon lamp was utilized to monitor absorbance at 372 nm. A solution of 0.2 M NaOH was filtered twice using a 0.45 micron Nalgene filter (Rochester, NY) prior to use. Compound **1** was dissolved in 18 M water. After mixing, each sample was collected; the pH values of the samples were measured using an InLab 412 pH electrode with an HA glass membrane that can withstand high pH (Mettler Toledo, Columbus, OH).

The parent naphthalene diimide (NDI) derivatives were synthesized using naphthalene-1,4,5,8-tetracarboxylic dianhydride (Alfa Aesar, Ward Hill, MA) with the appropriate amine: *N,N*-di-*n*-propyl-ethylenediamine (Karl Industries, Aurora, OH), 2-(*N*-piperidino)ethylamine (Karl Industries), 4-(2-aminoethyl)morpholine (Alfa Aesar), *N*-(2-aminoethyl)pyrrolidine (Alfa Aesar), 1-(3-aminopropyl)pyrrolidine (Alfa Aesar), and *N*-(3-aminopropyl)morpholine (Fisher). Toluene (99.9%, Fischer Scientific, Fair Lawn, NJ) was used as the solvent.

The parent NDIs were left unrecrystallized and each derivative was directly alkylated using iodomethane (Aldrich) in the indicated solvent. The purity of the derivatives was determined using ¹H NMR.

***N,N'*-Bis[1-(3-pyrrolidinyl)propyl]-1,4,5,8-naphthalenetetracarboxylic-1,8:4,5-diimide.** Naphthalene-1,4,5,8-tetracarboxylic dianhydride (0.6 g, 2.5 mmol) and *N*-(3-aminopropyl)pyrrolidine (1.2 g, 9.6 mmol) were mixed in toluene (75 ml) and allowed to reflux with a Dean-Stark trap for 3 h. The orange brown mixture was filtered and the

filtrate was removed under vacuum. The orange solid was recrystallized from ethanol and dried. $^1\text{H NMR}$ (CHCl_3): 1.65 [t, 8H, $\text{N}(\text{CH}_2\text{CH}_2\text{CH}_2\text{CH}_2)$], 1.98 [m, 4H, $\text{NCH}_2\text{CH}_2\text{CH}_2\text{N}(\text{CH}_2)_4$], 2.48 [t, 8H, $\text{N}(\text{CH}_2\text{CH}_2\text{CH}_2\text{CH}_2)$], 2.61 [t, 4H, $\text{NCH}_2\text{CH}_2\text{CH}_2\text{N}(\text{CH}_2)_4$], 4.30 [t, 4H, $\text{NCH}_2\text{CH}_2\text{CH}_2\text{N}(\text{CH}_2)_4$], 8.75 (s, 4H, Ar).

***N,N'*-Bis[1-(3-*N*-pyrrolidinyl-*N*-methyl)propyl]-1,4,5,8-naphthalenetetracarboxylic 1,8:4,5-diimide.** *N,N'*-Bis[1-(3-pyrrolidinyl)propyl]-1,4,5,8-naphthalenetetracarboxylic-1,8:4,5-diimide (66 mg, 0.13 mmol) was dissolved in chloroform (40 ml). Iodomethane (3.4 g, 27 mmol) was added to the dark brown solution which was allowed to stir overnight at room temperature. A precipitate formed and it was filtered under vacuum and washed with chloroform to give an orange-red solid. $^1\text{H NMR}$ (D_2O): 2.19 [m, 8H, $\text{N}^+(\text{CH}_2\text{CH}_2\text{CH}_2\text{CH}_2)$], 2.19 [t, 8H, $\text{NCH}_2\text{CH}_2\text{CH}_2\text{N}^+$], 2.96 [s, 6H, N^+CH_3], 3.45 [t, 4H, $\text{NCH}_2\text{CH}_2\text{CH}_2\text{N}^+$], 3.45 [t, 8H, $\text{N}^+(\text{CH}_2\text{CH}_2\text{CH}_2\text{CH}_2)$], 4.14 [t, 4H, $\text{NCH}_2\text{CH}_2\text{CH}_2\text{N}^+$], 8.51 [s, 4H, Ar].

***N,N'*-Bis[(2-*N*-pyrrolidinyl-*N*-methyl)ethyl]-1,4,5,8-naphthalenetetracarboxylic 1,8:4,5-diimide.** To a mixture of *N,N'*-bis[2-(*N*-pyrrolidinyl)ethyl]-1,4,5,8-naphthalenetetracarboxylic-1,8:4,5-diimide (0.10 g, 0.22 mmol) and acetonitrile (10 ml), iodomethane (4.6 g, 32 mmol) was added. After a few minutes, the orange-yellow mixture turned into a red-orange solution which was allowed to stir overnight at room temperature. A precipitate formed and was filtered under vacuum and washed with acetonitrile to give an orange solid. $^1\text{H NMR}$ (D_2O): 2.46 [t, 8H, $\text{N}^+(\text{CH}_2\text{CH}_2\text{CH}_2\text{CH}_2)$], 3.47 [s, 6H, N^+CH_3], 3.86 [t, 8H, $\text{N}^+(\text{CH}_2\text{CH}_2\text{CH}_2\text{CH}_2)$], 3.86 [t, 4H, $\text{NCH}_2\text{CH}_2\text{N}^+$], 4.86 [t, 4H, $\text{NCH}_2\text{CH}_2\text{N}^+$], 8.97 (s, 4H, Ar).

***N,N'*-Bis[(2-*N,N*-dipropyl-*N*-methylamino)ethyl]-1,4,5,8-naphthalenetetracarboxylic 1,8:4,5-diimide.** *N,N'*-Bis[(2-*N,N*-dipropylamino)ethyl]-1,4,5,8-

naphthalenetetracarboxylic-1,8:4,5-diimide (0.12 g, 0.22 mmol) was dissolved in chloroform (10 ml) and iodomethane (4.6 g, 32 mmol) was added. The dark brown solution was allowed to stir overnight at room temperature. A precipitate formed and was filtered under vacuum and was washed with chloroform and the resulting solid was dark red in color. $^1\text{H NMR}$ (D_2O): 1.21 [m, 12H, $\text{N}^+(\text{CH}_2\text{CH}_2\text{CH}_3)_2$], 2.06 [m, 8H, $\text{N}^+(\text{CH}_2\text{CH}_2\text{CH}_3)_2$], 3.39 [s, 6H, N^+CH_3], 3.59 [t, 8H, $\text{N}^+(\text{CH}_2\text{CH}_2\text{CH}_3)_2$], 3.79 [t, 4H, $\text{NCH}_2\text{CH}_2\text{N}^+$], 4.77 (t, 4H, $\text{NCH}_2\text{CH}_2\text{N}^+$), 8.94 (s, 4H, Ar).

***N,N'*-Bis[(2-*N*-piperidinyl-*N*-methyl)ethyl]naphthalene-1,4,5,8-bis(dicarboximide).**

N,N'-Bis[(2-*N*-piperidinyl)ethyl]-1,4,5,8-naphthalenetetracarboxylic-1,8:4,5-diimide (0.11 g, 0.23 mmol) was dissolved in chloroform (20 ml). Iodomethane (4.6 g, 32 mmol) was added to the light brown solution which was allowed to stir overnight at room temperature. A precipitate formed and was filtered under vacuum and was washed with chloroform to give a purple solid. $^1\text{H NMR}$ (D_2O): 1.90 [m, 4H, $\text{N}^+(\text{CH}_2\text{CH}_2\text{CH}_2\text{CH}_2)$], 2.16 [m, 8H, $\text{N}^+(\text{CH}_2\text{CH}_2\text{CH}_2\text{CH}_2\text{CH}_2)$], 3.47 [s, 6H, N^+CH_3], 3.66 [t, 8H, $\text{N}^+(\text{CH}_2\text{CH}_2\text{CH}_2\text{CH}_2\text{CH}_2)$], 3.89 [t, 4H, $\text{NCH}_2\text{CH}_2\text{N}^+$], under D_2O peak [t, 4H, $\text{NCH}_2\text{CH}_2\text{N}^+$], 8.99 (s, 4H, Ar).

***N,N'*-Bis[2-(4-morphyl-*N*-methyl)propyl]-1,4,5,8-naphthalenetetracarboxylic-1,8:4,5-**

diimide. *N,N'*-Bis[2-(4-morpholinyl)propyl]-1,4,5,8-naphthalenetetracarboxylic-1,8:4,5-diimide (0.12 g, 0.25 mmol) and was suspended in acetonitrile (10 ml). Iodomethane (2.3 g, 16 mmol) was added to the orange mixture and was allowed to stir overnight at 60 °C. The mixture was filtered under vacuum and was washed with acetonitrile to give a

red-orange solid. $^1\text{H NMR (D}_2\text{O)}$: 3.72 [s, 6H, N^+CH_3], 3.96 [t, 8H, $\text{N}^+(\text{CH}_2\text{CH}_2\text{OCH}_2\text{CH}_2)$], 4.10 [t, 4H, $\text{NCH}_2\text{CH}_2\text{N}^+$], 4.41 [t, 8H, $\text{N}^+(\text{CH}_2\text{CH}_2\text{OCH}_2\text{CH}_2)$], 4.95 [t, 4H, $\text{NCH}_2\text{CH}_2\text{N}^+$], 9.09 (s, 4H, Ar).

***N,N'*-Bis[(3-morpholinyl-*N*-methyl)propyl]-1,4,5,8-naphthalenetetracarboxylic**

1,8:4,5-diimide. *N,N'*-Bis[(3-morpholinyl)propyl]-1,4,5,8-naphthalenetetracarboxylic

1,8:4,5-diimide (0.47 g, 0.91 mmol) and was dissolved in chloroform (60 ml).

Iodomethane (4.6 g, 32 mmol) was added to the red-orange mixture and was allowed to stir at 60 °C for 2 days. The mixture was evaporated and washed with hot water (10 ml).

A yellow solid, similar to unalkylated NDI, was filtered and the filtrate was collected and allowed to crystallize. The crystals were filtered to give a yellow solid. $^1\text{H NMR (D}_2\text{O)}$:

2.64 [m, 4H, $\text{NCH}_2\text{CH}_2\text{CH}_2\text{N}^+$], 3.57 [s, 6H, N^+CH_3], 3.79 [t, 8H, $\text{N}^+(\text{CH}_2\text{CH}_2\text{OCH}_2\text{CH}_2)$], 3.90 [t, 4H, $\text{NCH}_2\text{CH}_2\text{CH}_2\text{N}^+$], 3.90 [t, 8H, $\text{N}^+(\text{CH}_2\text{CH}_2\text{OCH}_2\text{CH}_2)$], 4.60 [t, 4H, $\text{NCH}_2\text{CH}_2\text{CH}_2\text{N}^+$], 9.09 (s, 4H, Ar).

1.3 RESULTS

1.3.1 Synthesis

The NDI derivatives (Figure 1.1) were synthesized via condensation of one equivalent of naphthalene-1,4,5,8-tetracarboxylic dianhydride and two equivalents of the starting amine. The mixture was refluxed in toluene using a Dean Stark trap for 3 h.

The NDI derivatives were alkylated with iodomethane. Solvents including acetonitrile, chloroform, DMF and ethanol were used. Generally, the best results were achieved with a large excess of iodomethane in chloroform with stirring overnight at room temperature.

The morpholine derivatives, however, alkylated more slowly in chloroform. After

stirring overnight at room temperature, the CH₂CH₂-morpholine derivative gave a mixture of the dialkylated (**4**, singlet at 8.96 ppm) and the monoalkylated (AB quartet at 8.83 ppm) products, as seen from appropriate peaks in the ¹H NMR spectrum. Consistent with the NMR spectra, capillary electrophoresis (CE) showed two peaks at 15.8 min and 16.4 min with baseline separation. Complete alkylation for the CH₂CH₂-morpholine derivative was achieved in acetonitrile with a large excess of iodomethane at 60 °C for 12 h.³⁴ For the CH₂CH₂CH₂-morpholine derivative, complete dialkylation did not occur after two days in a large excess of CHCl₃ and iodomethane at 60 °C. The dialkylated product was dissolved in hot deionized water and the residue (unalkylated and partially alkylated material) removed by filtration.

1.3.2 UV-visible absorbance spectroscopy

The hydrolysis of the rings of **1** was followed by UV-visible absorbance spectroscopy. The starting diimide had two bands at 360 and 380 nm. In a borate buffer solution at pH 9.0, these bands decreased in intensity over time with three isosbestic point at 271, 306, and 352 nm (Figure 1.2).

In a second experiment, increments of NaOH were added to a sample in 50 mM phosphate buffer to give pH values of 8.0 - 13.1. As the base was added, the spectra were first seen to change from the diimide to a species with a broad peak from 350 to 370 nm, assigned as the monoimide (Figure 1.3). Further addition of base gave conversion of the monoimide to the diamide, with a peak centered at 308 nm. An isosbestic point at 326 nm was observed for this second transition. The maximum concentration of the monoimide occurred at pH 10.2. Figure 1.4 shows the spectra of the diimide, monoimide, and diamide.

A series of solutions of **1** were prepared at pH values ranging from 7.5 - 12.3. In each case, the system was allowed to reach equilibrium. Figure 1.5 shows the percentages of the three species as a function of the pH of the solution. The K_a values for conversion of the diimide to the monoimide (K_{a1}) and monoimide to the diamide (K_{a2}) were $2.5 \pm 0.2 \times 10^5 \text{ M}^{-1}$ and $2.0 \pm 0.1 \times 10^2 \text{ M}^{-1}$, respectively. A similar experiment was performed for **5**, in which the cationic charge is separated by an additional methylene group from the imide center. The K_a values were $1.4 \pm 0.1 \times 10^5 \text{ M}^{-1}$ and $44 \pm 2 \text{ M}^{-1}$, respectively.

1.3.3 NMR and capillary electrophoresis studies

NMR spectra as a function of pH were consistent with the proposed structures of the three species. For example, the aromatic protons of the diimide **1** appeared as a singlet at 8.97 ppm in D_2O . At a pH of approximately 12, the monoimide was seen as two sets of doublet of doublets from 7.62 ppm and 8.28 ppm (Figure 1.6). The diamide was seen as a series of six peaks at approximately 7.4 ppm. Two singlets at 7.39 and 7.43 ppm were ascribed to the *syn* isomer. An AB-quartet centered at 7.4 ppm with a coupling constant of 7.2 Hz was ascribed to the *anti* isomer. At 30 °C the compound was a 44/56 mixture of the *syn* and *anti* isomers. In addition to the peaks above, small amounts of unidentified hydrolysis products were observed. When the NMR tube was allowed to stand at room temperature for five days, it was found that the pH had decreased and that the monoimide concentration had increased. This observation was consistent with previous studies that ring opening is reversible.^{52,53}

A sample of **1** at pH 9.0 was also evaluated by capillary electrophoresis with diode array detection. Only two peaks were seen in the electropherogram (Figure 1.7).

The peak with the shorter migration time was the diimide and that with the longer migration time was the monoimide as determined from their absorbance spectra.

1.3.4 Kinetics of ring hydrolysis: diimide to monoimide

The hydrolysis of **1** from the diimide to the monoimide was followed by UV-visible spectroscopy as a function of pH in borate buffer. At a pH of 9.6, the approximate half-life was 5 min. The observed rate constant k_{obs} , calculated from the change in absorbance at 380 nm, increased linearly with the concentration of hydroxide (Figure 1.8). Because the reaction is reversible, the kinetics are expressed in terms of the sum of the forward (k_1) and reverse (k_2) rate constants.

$$k_{\text{obs}} = k_1[\text{OH}^-] + k_2$$

A plot of k_{obs} vs. $[\text{OH}^-]$ gave a second order rate constant of $130 \pm 3 \text{ M}^{-1} \text{ s}^{-1}$. The intercept, corresponding to k_2 , was less than 10^{-4} s^{-1} . The reverse rate was also calculated from the forward rate and the percentages of diimide and monoimide given the experimental K_{a1} for the interconversion. The average k_2 for the five points shown in Figure 1.8 was $5.2 \pm 0.3 \times 10^{-4} \text{ s}^{-1}$. The similarity of these two methods of calculating k_2 indicates that the contribution of water itself to the hydrolysis of the NDI is small.

A similar measurement for homolog **5** (Figure 1.9) gave a second order rate constant of $20.0 \pm 0.4 \text{ M}^{-1} \text{ s}^{-1}$. The intercept was less than $2 \times 10^{-5} \text{ s}^{-1}$. The reverse rate calculated from k_1 and the equilibrium data was $7.5 \pm 1.2 \times 10^{-5} \text{ s}^{-1}$.

1.3.5 Kinetics of ring hydrolysis: monoimide to diamide

At the concentrations of hydroxide necessary to observe significant amounts of the diamide ($> 0.005 \text{ M}$), the hydrolysis reactions are too fast to measure by conventional UV-visible absorption spectroscopy. Therefore, the reaction was studied using a

stopped-flow spectrophotometer. Figure 1.10 shows a plot of the absorbance at 372 nm as a function of time at 0.1 M NaOH in the absence of buffer. This wavelength was chosen for easy visualization because the absorbance changes from the diimide to the monoimide and monoimide to diamide are the same. Data are the average of nine individual kinetic runs, fit to two consecutive first-order reactions. The observed rates for the first (k_{obs1}) and second (k_{obs2}) hydrolysis processes were $17.0 \pm 0.2 \text{ s}^{-1}$ and $53.0 \pm 0.1 \times 10^{-2} \text{ s}^{-1}$, respectively.

1.4 DISCUSSION

1.4.1 The kinetics and equilibria of ring opening

In this work, we have compared the ring opening reactions of **1** and **5**. The conversion of the diimide to the monoimide is approximately 7-fold faster for the compound with the charge closer to the NDI central core; the half-lives at pH 9.6 are about 5 min (Figure 1.11) and 30 min (Figure 1.12), respectively. The faster reaction of the compound with the cationic charge closer to the imide is presumably due to electrostatic stabilization of the negatively charged transition state.

Equilibrium studies show that **1** converts from the diimide to the monoimide with a K_{a1} of $2.5 \pm 0.2 \times 10^5 \text{ M}^{-1}$ and from the monoimide to the diamide with a K_{a2} of $2.0 \pm 0.1 \times 10^2 \text{ M}^{-1}$. Expressed as apparent $\text{p}K_{\text{a}}$ values, these are 8.61 and 11.8, respectively. The conversion from the diimide to the monoimide for NDI **5** was K_{a1} of $1.4 \pm 0.1 \times 10^5 \text{ M}^{-1}$ and from the monoimide to the diamide with a K_{a2} of $44 \pm 2 \text{ M}^{-1}$, respectively. Expressed as apparent $\text{p}K_{\text{a}}$ values, these values are 8.8 and 12.4, respectively.

Comparison of the equilibria for **1** and **5** shows that the ring-opened form of **1** is favored by a factor of 1.8 for the first hydrolysis and 4.5 for the second hydrolysis.

Our work may be compared with that of Kheifets and Martyushina.⁵² They reported an apparent pK_a of 9.3 for the NDI with $\text{CH}_2\text{CH}_2\text{CH}_2\text{CH}_2\text{CH}_2\text{CO}_2^-$ side chains. They also reported that neither the NDI with positively charged ($\text{CH}_2\text{CH}_2\text{CH}_2\text{N}^+\text{Me}_3$) or with negatively charged ($\text{CH}_2\text{CH}_2\text{CH}_2\text{SO}_3^-$) aliphatic side chains showed ring-opened forms at pH 7.5. In our study, **1** is about 3% in the ring-opened form at pH 7.5. Thus, although the extent of ring opening is small, the NDI is interconverting between the ring-closed and ring-opened forms at physiological pH.

Aliphatic NDI derivatives are significantly more stable toward base than their aromatic counterparts. For example, the dicationic NDI with *N*-ethylpiperdinyphenyl [$-\text{C}_6\text{H}_4-\text{N}^+(\text{Et})\text{C}_5\text{H}_{10}$] side chains was about half converted to the monoimide at pH 6.7.⁵² The monoimide in turn was about half converted to the diamide at about pH 9.9. The corresponding apparent pK_a values for the hydrolyses of the dianionic NDI ($-\text{C}_6\text{H}_4-\text{SO}_3^-$ side chains) were 7.0 and 10.4. Thus, the presence of a cationic center in the side chain facilitates ring opening slightly in these systems; both are significantly more prone to ring opening in basic solution than are the aliphatic derivatives.

Our study is the first to measure the rate of ring opening of the monoimide to the diamide. At 100 mM, the rates of the first and second hydrolysis were $17.0 \pm 0.2 \text{ s}^{-1}$ and $53.0 \pm 0.1 \times 10^{-2} \text{ s}^{-1}$, respectively. Thus, the first reaction is about 30 times faster than the second. A recent study of the hydrolysis of naphthalene-1,4,5,8-tetracarboxylic dianhydride also showed that the first hydrolysis was faster than the second; in this case the difference was approximately a factor of 190.⁵⁷

The rates for ring closure were $7.5 \pm 1.2 \times 10^{-5} \text{ s}^{-1}$ for conversion of the diamide to the monoimide and $5.2 \pm 0.3 \times 10^{-4} \text{ s}^{-1}$ for conversion of the monoimide to the diimide. Thus, the second closure is about seven times faster than the first. The ring closure rate constants calculated from the intercept of the plot and from the on rate and the equilibrium constant are similar, indicating that contribution of water itself to the hydrolysis of the NDI is small. A similar conclusion regarding the participation of water in the hydrolysis was reached earlier.⁵³ A minimal contribution of water has also been shown in the hydrolysis of the naphthalene-1,4,5,8-tetracarboxylic dianhydride.⁵⁷

Borate can sometimes act as a catalyst in hydrolysis reactions.⁵⁸ To determine whether borate played a role in hydrolysis of the diimide, expected rates of ring opening at low pH (UV-visible range of experiments) were calculated from that measured at pH 13 with hydroxide alone (stopped-flow experiment). These calculated rate constants were in each case within 30% of the measured rate constants, arguing that borate does not catalyze the ring opening in this diimide system.⁵³

1.4.2 *Syn* and *anti* isomers of the diamide

NMR spectroscopy allowed visualization of all three species in solution. In previous work, Kheifets and Martyushina recorded NMR spectra of an aromatic NDI as a function of pH.⁵² Data were difficult to interpret, however, due to the overlap of the naphthalene protons and the side chain protons at the field then available (100 MHz). In the current study, the NMR of **1** at 600 MHz allowed clear visualization of each of the aromatic peaks. The diimide and monoimide were the expected singlet and AB quartet, respectively. The diamide showed a series of six overlapping peaks, all of which were resolved at 600 MHz. The spectra were consistent with a mixture of the *syn* and *anti*

isomers of this compound. To our knowledge, this is the first report of both isomers. The amounts of the *syn* and *anti* isomers are similar, indicating that there is very little energy difference between these two species.

NMR taken over time showed that this reaction was freely reversible, as has been found previously.⁵³ Reversibility of a monoimide ring opening has also been observed.⁵⁹

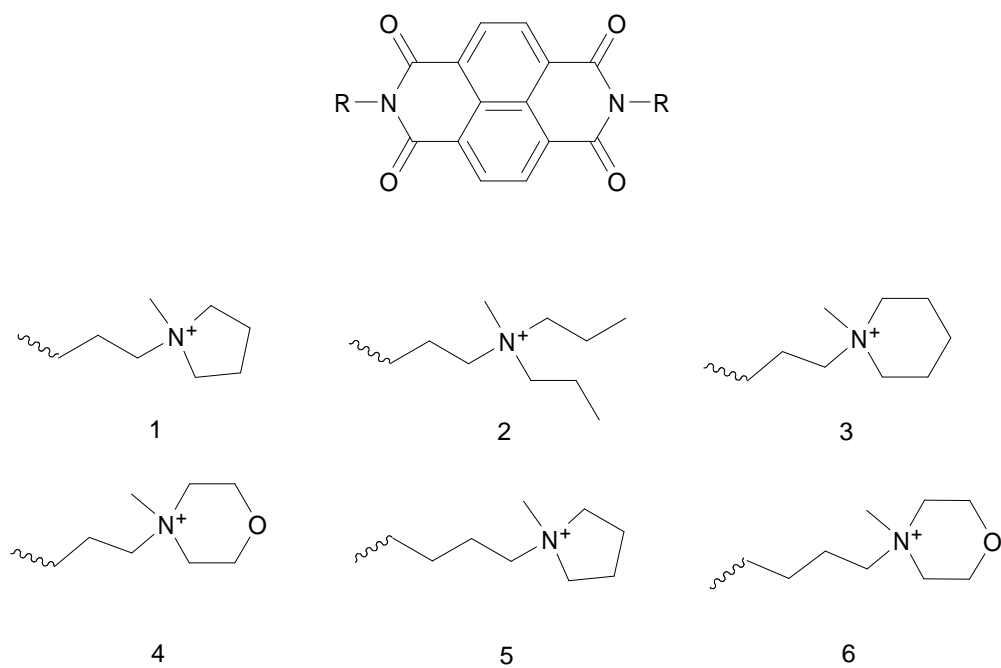


Figure 1.1 NDI derivatives in this study.

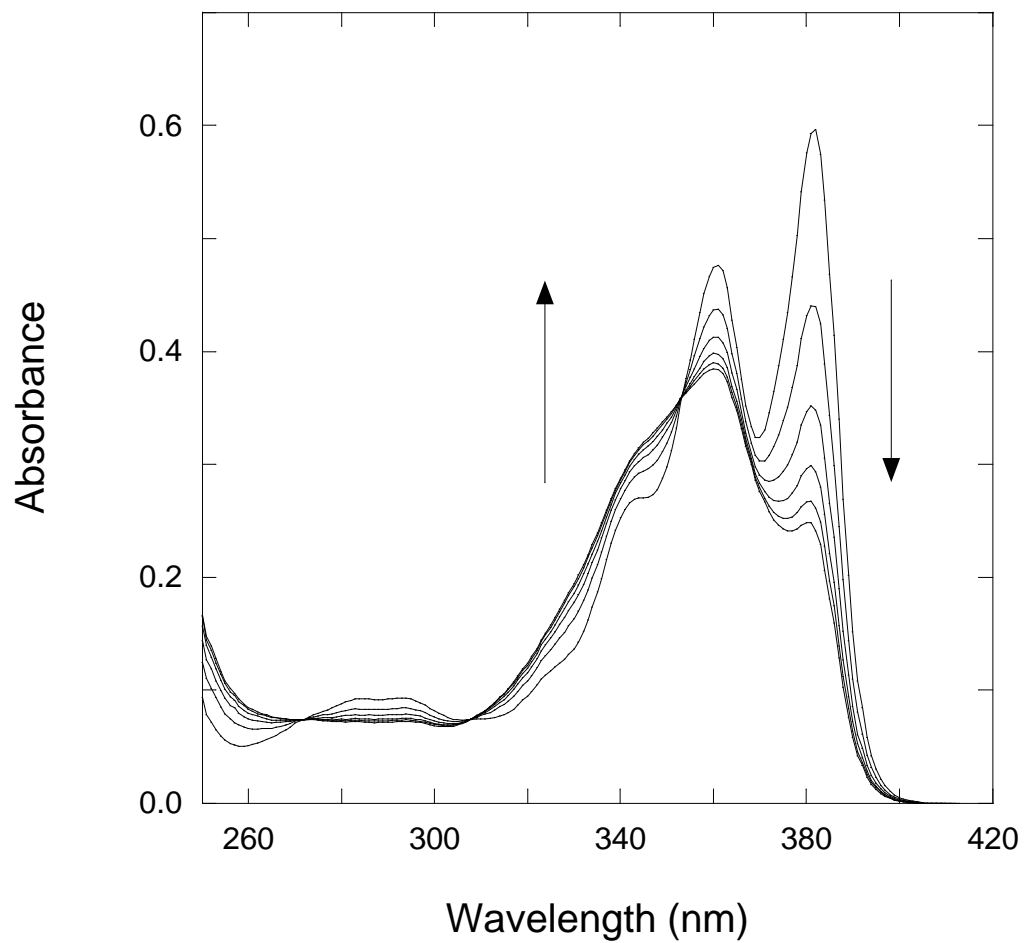


Figure 1.2. UV-visible absorbance spectra of **1** as a function of time (50 mM borate buffer at pH 9.0 with scans taken every 10 min for 50 min).

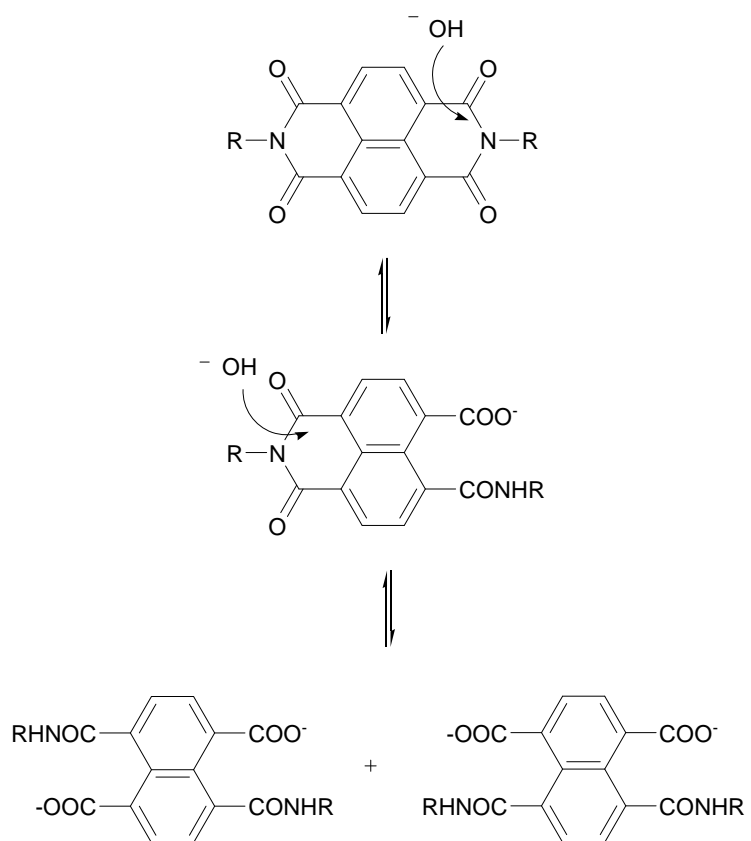


Figure 1.3. Mechanism of base-catalyzed hydrolysis of naphthalene diimides.

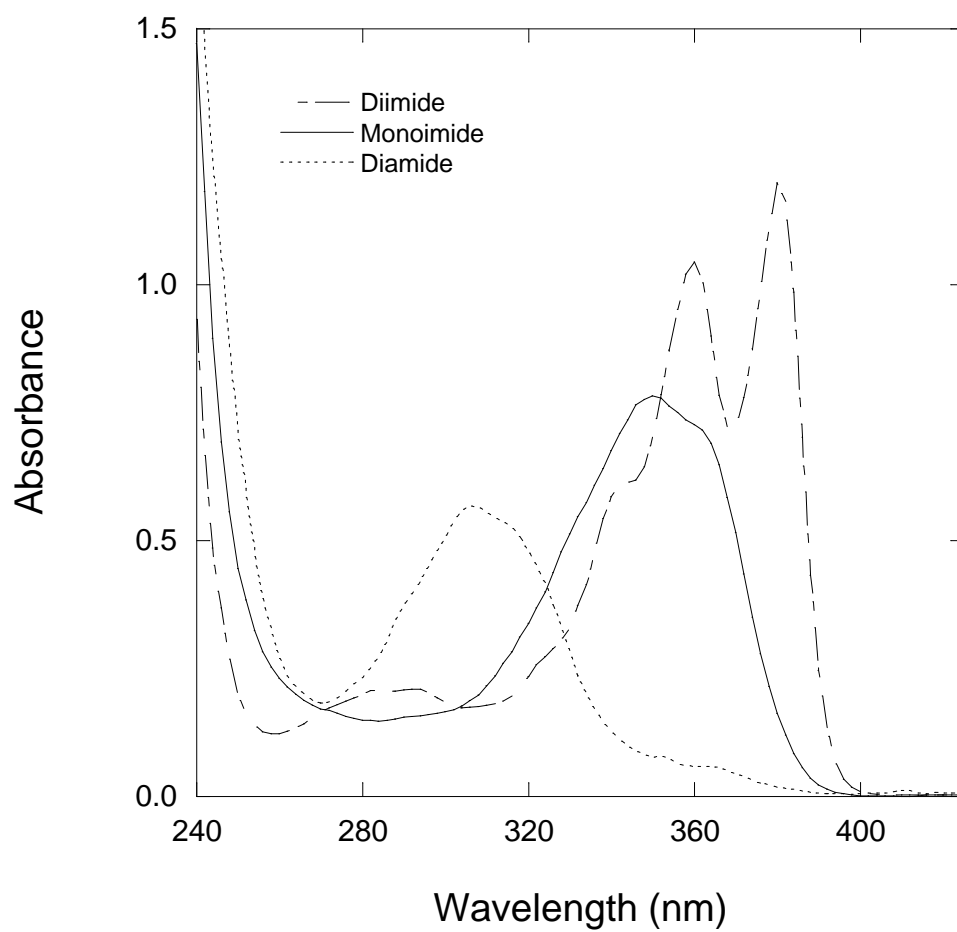


Figure 1.4. UV-visible spectra of the diimide, monoimide, and diamide.

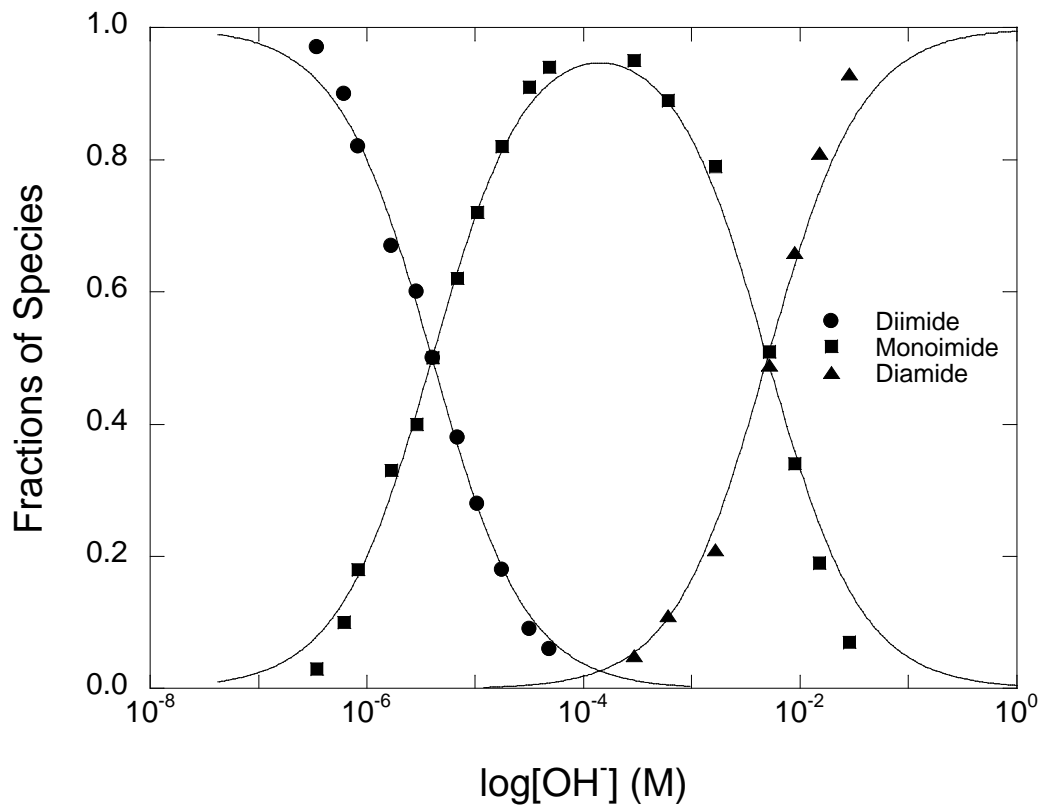


Figure 1.5. Fractions of the diimide, monoimide and diamide as a function of pH. Samples of **1** were equilibrated in a buffer containing 100 mM sodium phosphate and 100 mM sodium tetraborate.

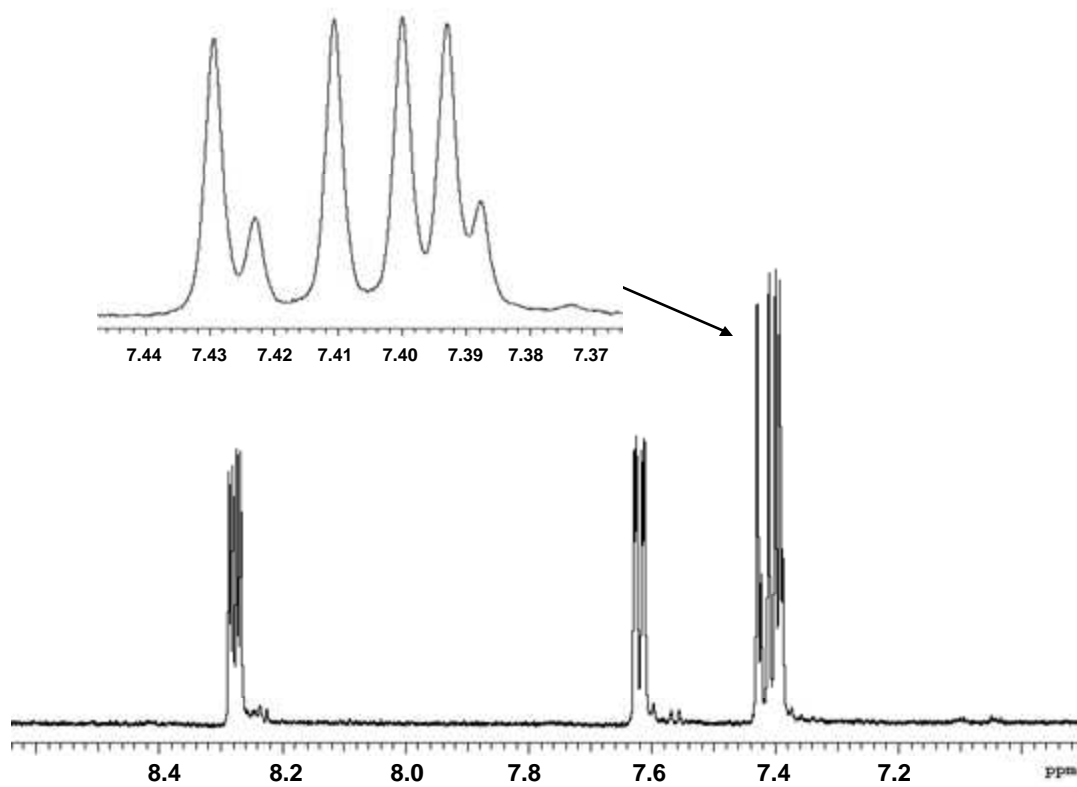


Figure 1.6. ^1H NMR at 600 MHz of compound **1** in D_2O at pH 12. The inset is the set of peaks at 7.4 ppm which is the diamide species (see text).

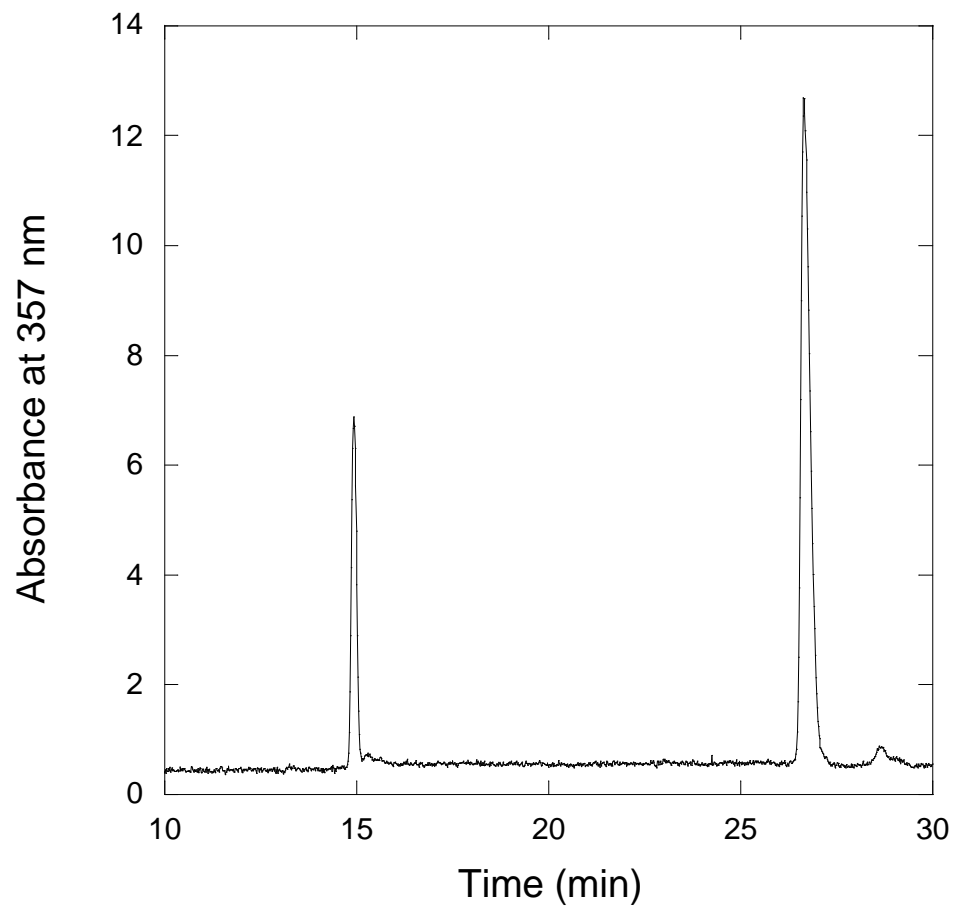


Figure 1.7. Electropherogram of NDI **1** (15.0 min) and its monoimide (28.6 min) using 25 mM sodium tetraborate buffer, pH 9.0, 11 kV.

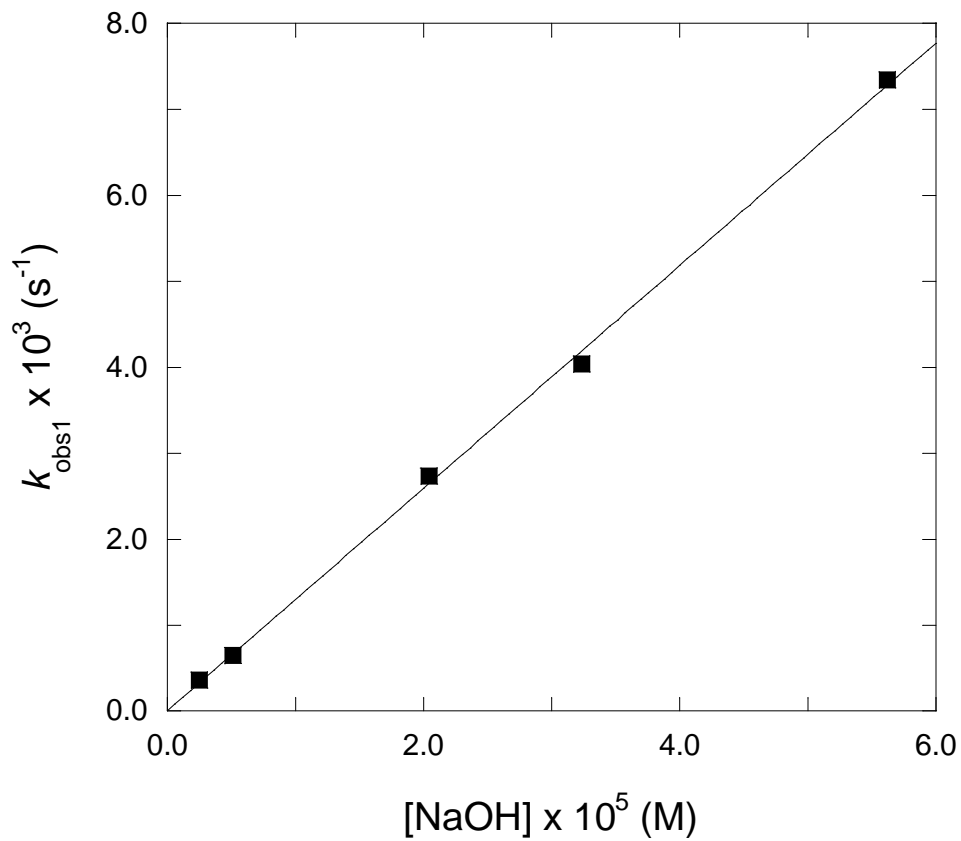


Figure 1.8. Rates as a function of the concentration of hydroxide for the first hydrolysis of NDI **1**. Reactions were run at 25 °C in 100 mM sodium tetraborate buffer.

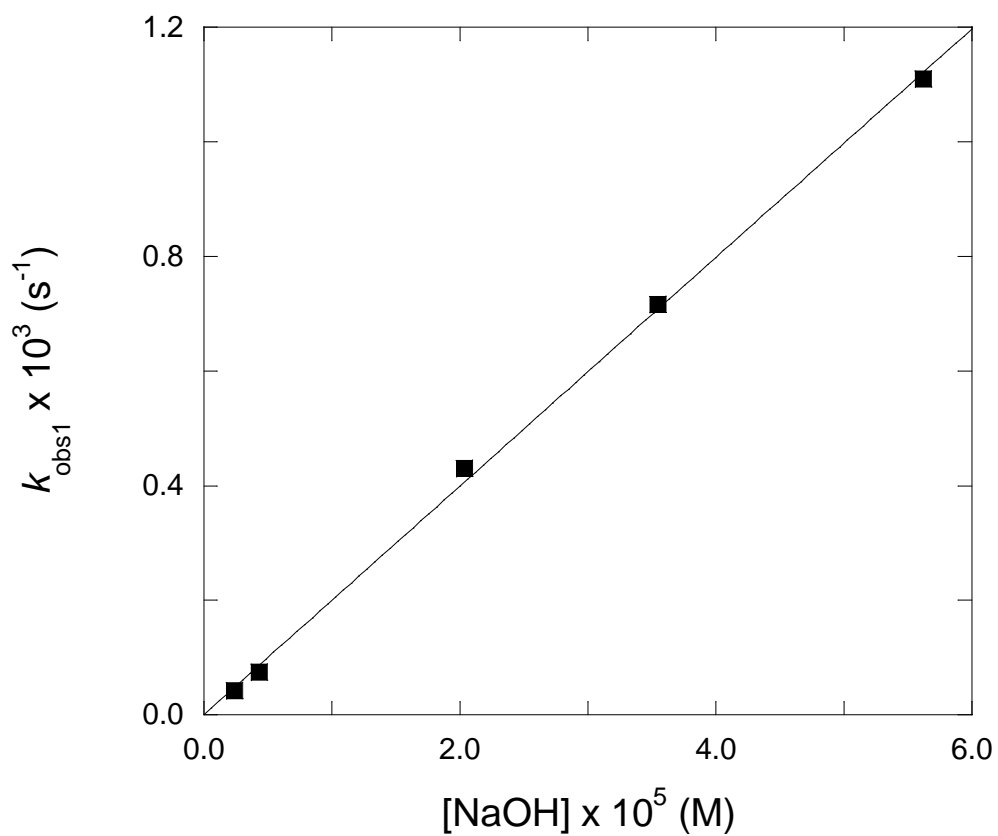


Figure 1.9. Rates as a function of the concentration of hydroxide for the first hydrolysis of NDI 5. Reactions were run at 25 °C in 100 mM borate buffer.

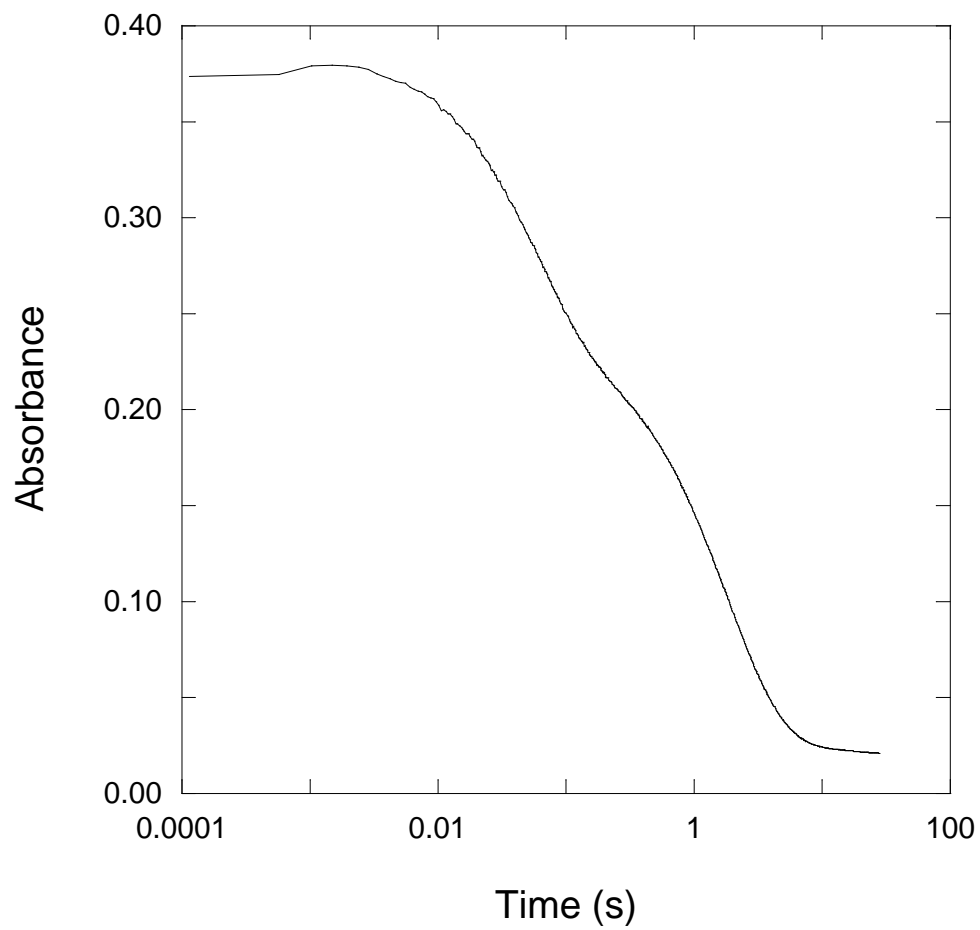


Figure 1.10. Stopped-flow trace of the absorbance of NDI **1** as a function of $\log(\text{time})$ in 100 mM NaOH. Data were taken at 372 nm.

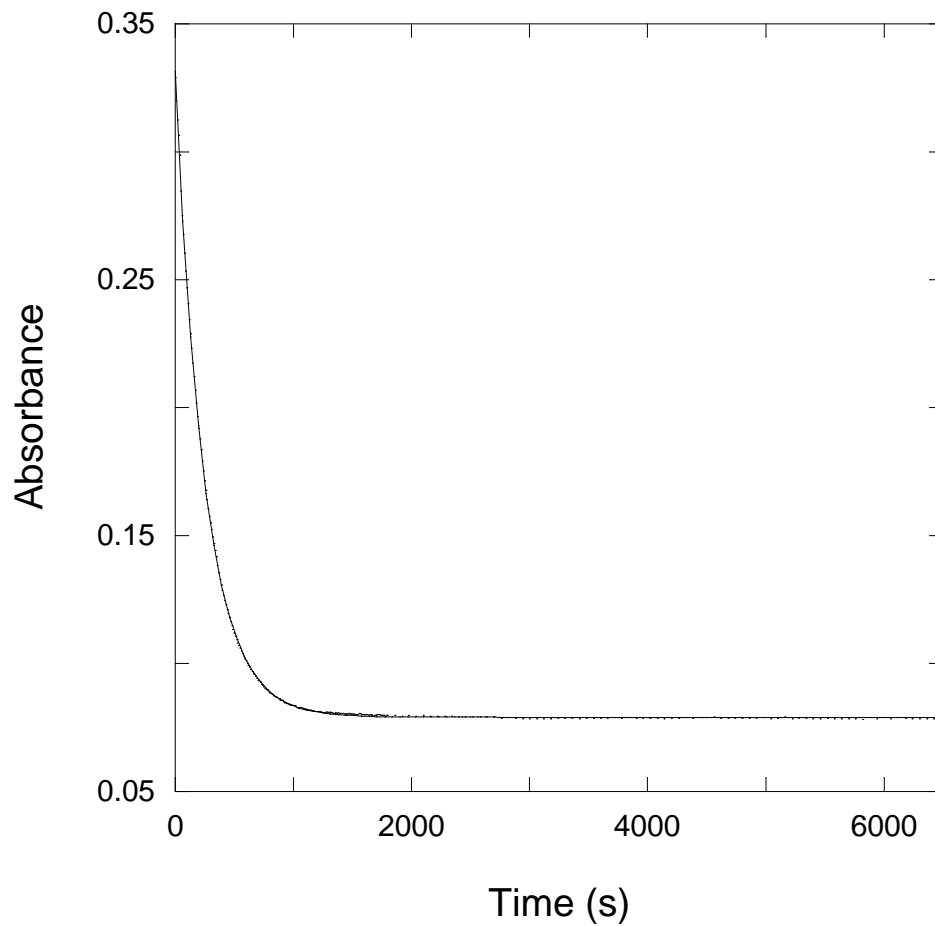


Figure 1.11. Absorbance as a function of time for **1** in 100 mM borate buffer at pH 9.6. The theoretical fit lies over the experimental points. Data were taken at 380 nm.

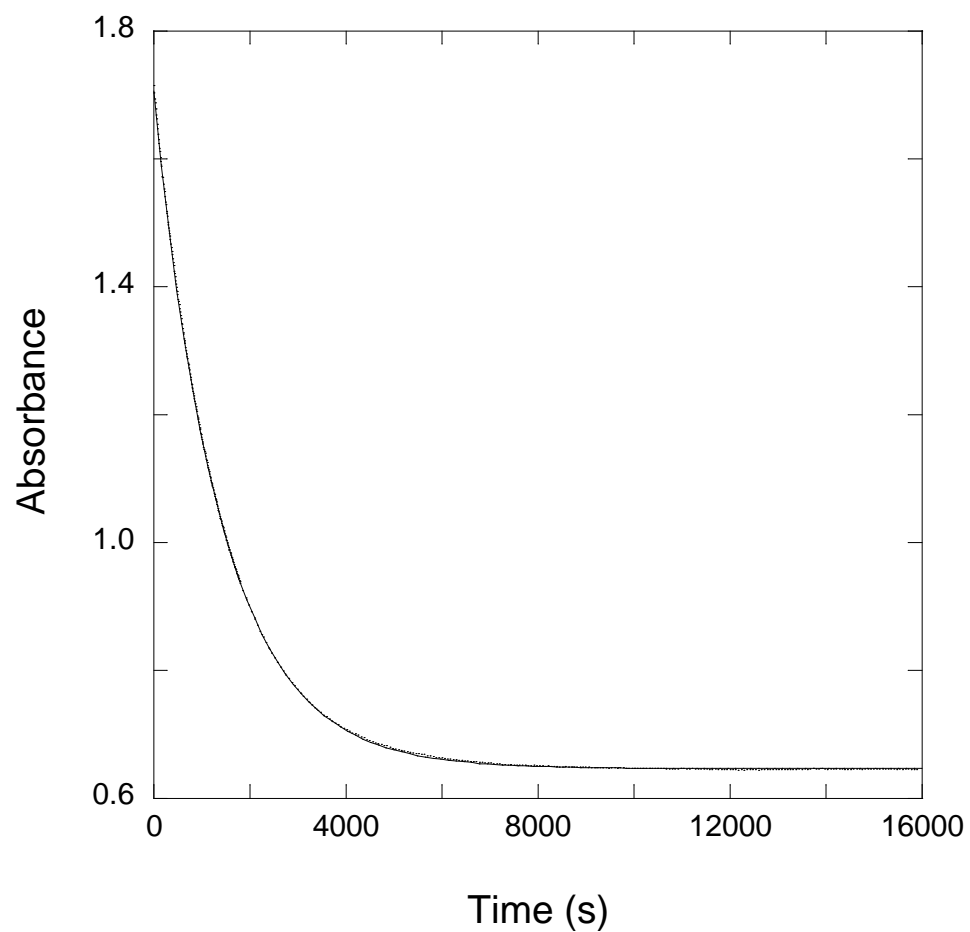


Figure 1.12. Absorbance as a function of time for **5** in 100 mM borate buffer at pH 9.6. The theoretical fit lies over the experimental points. Data were taken at 380 nm.

Chapter 2

2.0 Naphthalene diimides in chemistry. As detailed in Chapter 1, naphthalene diimides have many different roles in chemistry, in particular as redox reagents and in binding to nucleic acids. In conjunction with a study of the binding of these molecules to DNA, we synthesized four new NDI derivatives with cationic centers two atoms away from the central core. Molecules in this class have been synthesized before,^{3,19,22,50,51} but there has been no detailed study reported of the DNA binding of such derivatives.

In conjunction with these studies, it became apparent that our molecules could undergo ring opening very easily in base. Work done many years ago on NDI derivatives with charges further along the side chain from the central core had indicated that they were relatively stable in aqueous solution.^{52,53} No study of the compounds with the cationic center two atoms away had reported difficulties with spontaneous hydrolysis. However, our finding that these molecules are quite base sensitive led us to study the ring opening of these species in alkaline aqueous solution. To understand the effect of the position of the charge on hydrolysis, we also synthesized a derivative with the cationic charge three atoms away from the ring (**5**).

Chapter 2 begins by discussing additional details of the synthesis and spectroscopy of these species that were not elaborated in Chapter 1. We then turn to a discussion of the literature relevant to the hydrolysis of the NDI moiety and the related dianhydride. This includes a discussion of the possibility of buffer-catalyzed ring opening. Finally, we discuss additional aspects of the kinetic and equilibrium studies not presented in Chapter 1, particularly with regard to stopped-flow measurements.

2.1 Synthesis

2.1.1 Preparation of naphthalene diimides. The naphthalene derivatives were synthesized via a condensation reaction (Figure 2.1) using naphthalene-1,4,5,8-tetracarboxylic dianhydride (Alfa Aesar, Ward Hill, MA) with the appropriate propylamine: *N,N*-di-*n*-propyl-ethylenediamine (Karl Industries, Aurora, OH), 2-(*N*-piperidino)ethylamine (Karl Industries), 4-(2-aminoethyl)morpholine (Alfa Aesar), *N*-(2-aminoethyl)pyrrolidine (Alfa Aesar), 1-(3-aminopropyl)pyrrolidine (Alfa Aesar), and *N*-(3-aminopropyl)morpholine (Fisher). Toluene (99.9%, Fischer Scientific, Fair Lawn, NJ) was used as the solvent. The condensation reaction was achieved using a Dean-Stark trap that removed the water from the toluene-water which azeotropes. The purity of the derivatives was determined using ^1H NMR. The derivatives were directly alkylated using iodomethane (Aldrich) in the appropriate solvent and were not recrystallized.

2.1.2 Diethyl Derivative. The condensation reaction of the naphthalene with a primary amine is usually a colored reaction. Normally when heat is applied, the reaction will proceed from a dull color corresponding to the naphthalene dianhydride to a bright color. A color change did not occur for the diethyl derivative. UV-visible and infrared (IR) spectra were inconsistent with a naphthalene diimide. The UV-visible spectrum had peaks at 343 nm and 364 nm while the IR spectrum lacked key features indicative of the imide system such as an extra carbonyl band and almost all C-H bands. The only peaks visible were a weak band at 3079 cm^{-1} and 1763 cm^{-1} (data not shown). These spectra indicated that the reaction did not proceed to the desired product and this derivative was not pursued further.

2.1.3 Alkylation. The naphthalene diimide derivatives were alkylated using iodomethane following a number of different literature procedures. Methods from Steullet and Dixon were used where the NDI derivative was alkylated with a significant excess of iodomethane in a solvent at 60 °C for 12 h.⁴⁹ For example, the aminoethyldipropyl NDI **2** was alkylated on a 0.2 mmol scale in 10 ml of acetonitrile with 143 equivalents of iodomethane. The ¹H NMR spectrum showed that the product was the pure dialkylated NDI.

Alkylation was also attempted without heating.⁴⁹ The aminoethylpyrrolidine NDI (precursor to **1**) was alkylated using acetonitrile on a 0.2 mmol scale with 148 equivalents of iodomethane as the solvent; the mixture was allowed to stir for 12 h. A visible change in color from yellow-orange to dark red-orange was observed. The ¹H NMR indicated pure product. The aminopropylpyrrolidine derivative (precursor to **5**) was synthesized successfully in acetonitrile as well.

Overall, alkylation with iodomethane was most successful in chloroform at room temperature using a significant excess (63 to 560 equivalents) of iodomethane, with the exception of the two morpholine derivatives (discussed below). During alkylation, a notable color change occurred in many of the reactions. In general, those reactions which showed a color change also gave alkylated products. All NDIs in this study were soluble in water.

Alkylation of the aminoethylmorpholine NDI (precursor to **4**) was more difficult. An initial attempt involved DMF as the solvent at 60 °C for 12 h.⁴⁹ In this the reaction, 0.10 mmol of the precursor was dissolved in 10 ml of DMF and 560 equivalents of iodomethane were added. During heating, a color change from orange to red was

observed. NMR of the product showed chemical shifts in the aliphatic region consistent with alkylation, but impurity peaks in the aromatic region were present. Recrystallization from water did not give pure product. A second attempt involved 0.10 mmol of the precursor in 25 ml of diethyl ether with 6.3 mmol of iodomethane in the dark for 1 day at room temperature.⁶⁰ The material did not appear to go into solution and there was no observable color change. The NMR showed only starting material and no product. A third attempt involved 0.22 mmol of the precursor in 10 ml of a 1:1 solution of benzene and DMSO with 40 mmol iodomethane stirred overnight with no heat.⁶¹ The NMR showed only starting material. In a fourth attempt, 0.23 mmol of the precursor was alkylated in chloroform using 32.1 mmol of iodomethane for 12 h with no heat. A red precipitate was formed. The NMR showed that the precipitate was a mixture of the mono- and the dialkylated products (discussed in 2.1.4). The precursor was finally dialkylated with 10 ml of acetonitrile on a 0.3 mmol scale with a 63 equivalents of iodomethane. The mixture was covered and heated at 60 °C for 12 h. The NMR showed that dialkylation yielded **4**, but the compound contained small amounts of impurities.

2.1.4 Monoalkylated diimides. In a number of instances, attempted alkylation gave monoalkylated products. For example, Figure 2.2 shows the NMR spectrum of a mixture of the dialkylated (singlet at 8.96 ppm) and monoalkylated (AB quartet at 8.87 ppm) aminoethylmorpholine derivatives. The protons on the aromatic ring system, H_a and H_b, have slightly different chemical environments caused by the cationic charge. H_a will split H_b into a doublet while H_b will split H_a into a doublet. The result is an AB quartet with J = 7.8 Hz. The increased intensity of the inner peaks arises because chemical shift difference and the coupling constant are of similar magnitude.

Integration of the peaks showed that nearly an equal mixture of both dialkylated and monoalkylated species were present. Capillary electrophoresis (CE) was used to separate the two products. There were two peaks present in the electropherogram at 15.8 min and 16.4 min with baseline separation (Figure 2.3).

2.2 Literature studies

2.2.1 Hydrolysis of NDI. Kheifets and Martyushina studied the hydrolysis of naphthalene diimide derivatives with various substituents (Figure 2.4).⁵² Both imide rings of the diaryl NDI with $p\text{-C}_6\text{H}_4(\text{C}_2\text{H}_5)\text{N}^+\text{C}_5\text{H}_{10}$ substituents opened when the diimide was treated with base. Titration of the diimide with two equivalents of base showed a two step titration curve caused by the first and second imide ring opening processes. An initial UV-visible spectrum of the unhydrolyzed diaryl diimide had peaks at 362.5 and 382.5 nm. The monoimide species was observed when solutions of diimide in phosphate buffer between pH 6.0 and 8.2 at 37 °C were allowed to equilibrate for 24 h. The two peaks at 362.5 and 382.5 nm were seen to decrease into a broad peak around 350 nm with an isobestic point at 358 nm. As the pH was raised from 8.5 to 10.9, the peak at 350 nm decreased and the peak at 320 nm increased. There was an isobestic point at 335 nm. The transformation of the diimide to the monoimide occurred in the pH range of 6.0 to 8.3 while that of the monoimide to diamide occurred in the pH range of 8.5 to 10.5.

An NMR spectrum of the diimide was taken at 100 MHz in D₂O. At pH 4.0, a singlet from the protons on the naphthalene ring was seen at approximately 8.6 ppm. Two sets of doublets from the aromatic side chain at 7.5 to 8.3 ppm were seen as well. The pH was increased to 8.2 with the addition of an equivalent of base. The spectrum

showed a quartet at approximately 8.6 ppm and an increase in the number of peaks between 7.5 and 8.3 ppm. When the pH was increased to 10.2, the quartet merged with the aromatic protons upfield at 7.5 - 8.0 ppm. At pH 11.5, the spectrum showed a singlet at approximately 7.8 ppm.

The equilibria from the diimide to the monoimide to the diamide were shifted only slightly by the charge of the substituent. For example, the pK_a values of the conversion for the NDI bearing the negatively charged side chain $p\text{-C}_6\text{H}_4\text{SO}_3^-$ were 6.98 and 10.37, respectively. The positively charged side chain $p\text{-C}_6\text{H}_4(\text{C}_2\text{H}_5)\text{N}^+\text{C}_5\text{H}_{10}$ had pK_a values of 6.69 and 9.98, respectively. When the charge is insulated from the imide group undergoing hydrolysis by the phenyl ring, the effect of charge is comparatively small.

NDIs bearing dialkyl side chains are far less prone to ring open in base. The pK_a value of the first ring opening for the NDI with dialkyl $(\text{CH}_2)_3\text{N}^+(\text{CH}_3)_3$ side chains was 9.31. Kheifets and Martyushina stated that naphthalene diimides substituted with dialkyl functional groups did not hydrolyze at neutral pH values of 6 to 8.⁵²

2.2.2 Kinetics of the hydrolysis of NDI. Kheifets and Martyushina measured the kinetics (k_{obs}) of the first ring opening the NDI bearing the diaryl substituent $p\text{-C}_6\text{H}_4(\text{C}_2\text{H}_5)\text{N}^+\text{C}_5\text{H}_{10}$ in phosphate buffer.⁵³ The reaction was treated as a reversible equilibrium with terms for hydrolysis by water and hydroxide:

$$k_0 = k_{\text{H}_2\text{O}} + k_{\text{OH}^-} [\text{OH}^-] + k_{\text{rev}}$$

To account for any effect of catalysis by phosphate, the k_{obs} were measured at different concentrations of phosphate buffer at a given pH. When these k_{obs} were plotted with respect to phosphate concentration and the data extrapolated to the y-axis, the k_0 value was obtained for that pH. A series of k_0 values were plotted with respect to their corresponding hydroxide concentrations and the line was extrapolated to the y-axis to obtain the k_0 at zero phosphate buffer concentration (k_0'). Using the value found for k_0 , the $k_{\text{H}_2\text{O}} + k_{\text{rev}}$ value was found to be $5 \times 10^{-5} \text{ s}^{-1}$.

The k_{rev} value was calculated by using the equation $k_{\text{rev}} = k_f/K_{\text{app}}$, where $K_{\text{app}} = [\text{monoimide}]/[\text{diimide}]$. The k_{rev} value was $7 \times 10^{-5} \text{ s}^{-1}$. Comparison of this with the $k_{\text{H}_2\text{O}} + k_{\text{rev}}$ value indicated that $k_{\text{H}_2\text{O}}$ was negligibly small.

The rate of hydrolysis increased with increasing concentration of phosphate buffer. At a phosphate concentration of 0.150 M, the k_{obs} increased approximately from $1 \times 10^4 \text{ s}^{-1}$ to $13 \times 10^4 \text{ s}^{-1}$ from pH 6.4 to 7.9, respectively. At pH 7.9, increasing the concentration of phosphate from 0.0375 M to 0.150 M increased the k_{obs} from $9 \times 10^4 \text{ s}^{-1}$ to $13 \times 10^4 \text{ s}^{-1}$.

The rate of the first ring opening was measured for both positively and negatively charged NDI derivatives. At pH 7.5, the NDI with diaryl $p\text{-C}_6\text{H}_4(\text{C}_2\text{H}_5)\text{N}^+\text{C}_5\text{H}_{10}$ substituents had a k_f of $0.49 \times 10^3 \text{ M}^{-1}\text{s}^{-1}$ with a k_{rev} of $0.1 \times 10^3 \text{ s}^{-1}$. At the same pH, the NDI with $p\text{-C}_6\text{H}_4\text{SO}_3^-$ substituents had a k_f that was two-fold slower than its positive counterpart. The reverse rates were nearly the same for the two derivatives. As the pH increased from 9.7 to 10.2, the k_f for the positively charged NDI increased from 1.70 to $5.90 \times 10^3 \text{ M}^{-1}\text{s}^{-1}$. The k_f for the negatively charged NDI had a slightly smaller increase from 0.60 to $1.70 \times 10^3 \text{ M}^{-1}\text{s}^{-1}$ over the same pH range.

The half-lives for dialkyl substituted NDIs with three carbon linkers between the NDI core and the charged group on the side chain were measured in 200 mM borate buffer solution at pH 10.1 at 37 °C. The NDI with dialkyl substituents $(\text{CH}_2)_3\text{N}^+(\text{CH}_3)_3$, $(\text{CH}_2)_3\text{SO}_3^-$, and $(\text{CH}_2)_3\text{CO}_2^-$, had half-lives of 1, 6, and 14 min, respectively. The data show that positively charged NDI substituents, whether diaryl or dialkyl, increase the rates of hydrolysis.

2.2.3 Diimide-lactam rearrangement. Hydrolysis is not the only pathway that the diimide can take when it reacts with an alkali metal hydroxide. In alcohol, a rearrangement of the diimide can occur. Langhals and von Unold studied the lactam rearrangement in naphthalene diimides and perylene diimides.^{55,56} Rearrangement of six-membered diimide rings was observed when the diimide was treated with KOH/*tert*-butyl alcohol. Two hydrolysis products (anhydride and diacid) were the result, but small amounts of the lactamimide were seen. Carbon dioxide was lost during the rearrangement, which contracted the ring, forming a lactamimide.

When *tert*-butyl alcohol was replaced with methanol or ethanol, the lactamimide was the major product. The addition of DMSO to the mixture increased the yield of the lactam products and decreased the length of reaction. Although the lactam was the major product, trace amounts of hydrolysis products were still observed. A color change in the salt to orange-red or blue was a physical characteristic of the hydrolyzed product.

The rearrangement of the second imide ring does not occur even under harsh conditions. Langhals and von Unold found that the lactam rearrangement could only occur when a second imide ring was present. This was in agreement with the observation that the monoimide did not contract into a lactam.

2.2.4 Hydrolysis of naphthalene tetracarboxylic dianhydride. A recent study of hydrolysis of naphthalene-1,4,5,8-tetracarboxylic dianhydride⁵⁷ allows comparison of the kinetics of the diimide system with that of the dianhydride system. An initial spectrum of the unhydrolyzed dianhydride in water showed a λ_{max} at 368 nm and a second peak at 348 nm. When the dianhydride was dissolved in buffer solution at pH 7.0, the peak at 368 nm rapidly decreased with a half life of 24 s. A second, slower process also occurred with a half-life of 2 h, decreasing the peak at 368 nm further. The decrease at 368 nm was accompanied by an increase at 308 nm. An isobestic point was observed at 338 nm. The fast decrease at 368 nm was attributed to the hydrolysis of the dianhydride to the monoanhydride species. The slower process was attributed to the hydrolysis of the monoanhydride to the tetracarboxylic acid.

2.2.5 Possible buffer contribution to hydrolysis. In view of the sensitivity of the reaction to the pH, it was necessary to choose a robust buffer for these experiments. It was desirable that the buffer (a) have a wide range of buffering capacity, (b) be invisible in NMR studies and (c) not contribute to the hydrolysis either via a covalent intermediate or by acting as a general base.

Initially we began with a sodium phosphate buffer, because we did not want protons from the buffer to appear in the NMR spectra. NMR experiments herein are all reported in sodium phosphate buffer. It became clear, however, that it was difficult to hold the pH over the entire range needed with phosphate alone.

We then moved to phosphate-borate buffer, because this has been used previously with good success in NMR experiments over a fairly wide range of pH values. The phosphate buffered well around pH 7 - 8 and 11 - 12 while borate buffered well around

9 - 10 giving the mixture the capacity to buffer over a wide range. Optical equilibrium data are reported in this buffer.

We also tried glycine buffer, but the pH did not hold well. We tried 3-(cyclohexylamino)-1-propanesulfonic acid (CAPS) for the capillary electrophoresis separations, but perhaps as might be expected, the buffer seemed to be reacting with the compound as seen by multiple peaks and noise in the electropherogram. CE experiments were therefore performed in phosphate buffer.

It was also necessary to optimize conditions for the kinetics experiments. It has been shown that phosphate helps catalyze hydrolysis of diimides,⁵³ and therefore this buffer was not a good option. For the stopped-flow experiments, no buffer was used to eliminate any possible contribution of buffer to hydrolysis. However, as discussed below, in the absence of buffer, it was very difficult to be certain of the pH of the solution at the time of the hydrolysis.

We then considered borate buffer alone. The role of borate in catalyzing hydrolysis varies considerably from system to system. Borate can serve as an intramolecular catalyst by binding to a nearby oxygen in the structure (Figure 2.4).⁶²⁻⁶⁵ There are also examples in which borate catalyzes a reaction without this covalent intermediate, presumably by attaching itself to the hydrolytic center in some manner as shown in Figure 2.5.⁶⁶⁻⁶⁸ A study by Ernst and Schmir on the hydrolysis of isoimides indicated that borate played a significant role in the hydrolysis of this system (Figure 2.4).⁵⁸ One could imagine that borate could serve as a general base in a mechanism where the hydrolysis begins with a molecule of water attacking the imide ring (Figure 2.6). The borate molecule would then remove the proton from the intermediate. A molecule of

water would be lost, converting borate to $B(OH)_3$. Perrin has proposed, however, that borate should not be considered as a general acid/base catalyst.⁶⁹ There are still other instances in which borate does not seem to have a significant effect on rates of hydrolysis.^{69,70}

Although it had been reported that increasing borate concentration from 0.01 - 0.05 M had no significant effect on the rate of hydrolysis of diimides,⁵³ it seemed prudent to verify this in view of the many different experimental findings regarding borate's role in hydrolysis by various research groups. In line with Kheifets and Martyushina, we found that borate does not catalyze hydrolysis described in Chapter 1.

2.3 Experimental studies

2.3.1 Recording the spectrum of the monoimide. The UV-visible spectrum of the monoimide was first approximated in an experiment where increments of dilute NaOH were added to a sample of **1** in 50 mM phosphate buffer. The initial pH was 8.0. Increments of 0.5 μ L of NaOH were added to the cuvette and a spectrum was taken after each addition. As the base was added, bands at 360 and 380 nm decreased and a broad peak from 350 to 370 nm increased with an isosbestic point at 352 nm. The monoimide was taken as the last spectrum before the spectra were no longer isosbestic at 352 nm.

In the experiment above, the pH of the solution with the maximum amount of monoimide was measured as 10.7 (Figure 2.7). It was realized subsequently, however, that the solution had not been allowed to stand long enough to reach equilibrium after each addition. To find the pH at which the solution had the highest concentration of monoimide after equilibration, solutions of **1** in phosphate buffer were equilibrated

overnight at pH 9.5, 10.2, and 10.7. The spectrum at 10.2 was very close in appearance to the last spectrum that was still isosbestic as in the previous experiment. The spectrum at pH 10.2 was therefore used as the monoimide spectrum in the calculation of the percentages of each species derived from linear combinations of the three spectra.

Returning to the first experiment, further addition of base gave conversion of the monoimide to the diamide, with a peak centered at 308 nm. An approximate isosbestic point at 326 nm was observed for this second transition. As shown in Figure 2.8, a slight drift in wavelength was noted, which presumably indicates that a small percentage of diimide was still present in the solution. Concentrated NaOH was added at the end of the titration to ensure that conversion to diamide was complete (final two spectra).

2.3.2 Determination of K_a . As reported in Chapter 1, a series of solutions of **1** were prepared at pH values from 7.5 to 12.3. In each case the system was allowed to reach equilibrium. The fractions of species from the optical data of each solution were calculated from linear combinations of the spectra of the individual species. A nonlinear least squares fitting using the formula below⁷¹ was performed on the fraction of the monoimide as a function of pH to find the values of K_{a1} and K_{a2} .

$$[\text{monoimide}] = \frac{K_{a1}[\text{OH}^-]}{1 + K_{a1}[\text{OH}^-] + K_{a1}K_{a2}[\text{OH}^-]^2}$$

The K_a values for conversion of the diimide to the monoimide and monoimide to the diamide were $2.5 \pm 0.2 \times 10^5 \text{ M}^{-1}$ and $2.0 \pm 0.1 \times 10^2 \text{ M}^{-1}$, respectively. Since the K_a values were considerably different, the percentages of the three species as a function of the pH of the solution could be calculated using the formulas below (Figure 1.5).

$$K_{a1} = \frac{[\text{monoimide}]}{[\text{diimide}][\text{OH}^-]}$$

$$K_{a2} = \frac{[\text{diamide}]}{[\text{monoimide}][\text{OH}^-]}$$

Figure 1.4 shows the spectra of the diimide, monoimide, and diamide. The titration curves used to calculate the K_{a1} and K_{a2} for **5** are shown in Figure 2.10.

2.3.3 Attempted reclosing of the diimide. A sample of **1** in 50 mM phosphate buffer at pH 5.0 was treated with concentrated NaOH to give a solution with a peak at 308 nm, indicating that all of the diimide had converted to the diamide species. Aliquots of concentrated HCl were added to the solution (Figure 2.9). The peak at 308 nm shifted to 350 nm, indicating that a majority of the diamide had converted to the monoimide. With the addition of more acid, two peaks emerged at 339 and 354 nm. Increasing the amount of HCl in solution did not give the peaks at 360 and 380 nm associated with the diimide. Instead, the spectrum appeared to be more similar to that of the dianhydride. However, it is not only this species, which has peaks at 348 and 368 nm.⁵⁷ The reaction was not further investigated.

2.3.4 ¹H NMR spectroscopy. A singlet for the four aromatic protons between 8.0 and 9.0 ppm is characteristic of the NDI ring system. Each hydrolysis product also has a set of characteristic peaks because their protons have different splitting patterns in the NMR spectra. In Figure 2.11, the structure of the hydrolytic products is given with their protons labeled.

The 300 MHz NMR spectrum of the NDI **1** in D₂O had a singlet at 8.74 ppm. When NaOD was added, the monoimide was seen as two sets of doublet of doublets from 7.97 ppm and 8.62 ppm and the diamide as a series of six peaks at approximately 7.7 ppm (Figure 2.11). The six peaks for the diamide were not well-resolved. Therefore, a spectrum on the 600 MHz spectrometer was taken, allowing assignment of the peaks as an AB-quartet due to the *anti* isomer and two singlet peaks assigned to the *syn* isomer (Figure 1.6). The two products were formed in almost equal amounts, indicating that they are very similar energetically. To our knowledge, this is the first report of the *syn* geometry in this type of ring system. The spectrum was measured as a function of temperature to see if additional separation of the peaks could be achieved. At 30, 50, and 70 °C, the chemical shifts did not change significantly (Table 2.1).

When the sample was first investigated, it was 14/86 mixture of monoimide and diamide. After approximately five days, the pH had decreased to approximately 10 and the mixture had converted to a 93/7 ratio. This change of the monoimide/diamide ratio over time indicates that hydrolysis is reversible. This has been noted previously in this and related systems.^{52,53,72}

Compound **1** was dissolved in DMSO and a few drops of NaOD were added to the sample. The addition of the base changed the sample color from clear to red. At 400 MHz, the aromatic region showed a series of peaks (data not shown). The peaks were not readily interpretable in terms of the three species under discussion, and this study was not pursued.

2.3.5 Stopped-flow kinetics. Chapter 1 discusses the rate of the second hydrolytic process which was measured using a stopped-flow spectrometer. The $k_{\text{obs}1}$ and $k_{\text{obs}2}$, for the first and second hydrolysis processes were $161 \pm 8 \text{ s}^{-1}$ and $5.0 \pm 0.1 \text{ s}^{-1}$, respectively (Table 2.2). As mentioned in Chapter 1, the stopped-flow measurements were monitored at one wavelength. For ready visualization, it was desired to choose a wavelength where the change in absorbance for both hydrolytic processes was the same. To achieve this, two difference spectra were calculated. First, a difference spectrum was plotted by subtracting the diimide spectrum from the monoimide spectrum. Second, a difference spectrum was plotted by subtracting the monoimide spectrum from the diamide spectrum. These two difference spectra intersect at 372 nm (Figure 2.12), indicating equal optical changes for both hydrolytic processes at this wavelength.

In initial experiments, the probe used to measure the pH did not give accurate values. In extreme pH environments such as pH 13, pH probes can leach protons from the glass membrane. This leaching causes issues such as calibration difficulties, unstable pH readings, or large pH drifts. With continuous use at high pH, the leaching can render the probe useless. Soaking the probe in acidic solutions such as 0.1 M HCl or a buffer solution at pH 3 for 30 min to 1 h may stabilize the probe, but other times replacement of the probe may be necessary. A probe with a special membrane was used to measure the pH for the stopped-flow experiment. The HA (high alkali) membrane does not completely prevent leaching, but is robust enough to be used repeatedly at high pH.

The stopped-flow experiments were run without buffer in view of the concern that buffer would catalyze the reaction.⁵³ Absorbance as a function of time was recorded after mixing **1** in water and an unbuffered solution of NaOH. Hydroxide solutions were made

via serial dilutions starting at 100 mM NaOH (pH 13) (Figure 2.13, Table 2.3). The kinetic experiments were run from high to low pH, to attempt to condition the system starting with the highest concentration of hydroxide. To attempt to condition the lines, the syringes and lines were washed with new base solution approximately six times before each run.

The pH of each solution was measured after each run. Table 2.4 shows the expected concentrations of hydroxide calculated from the two-fold serial dilutions and the experimental pH values measured from the effluent of the stopped-flow experiments. After the first solution, the measured concentrations of hydroxide were lower than the theoretical concentrations. This is expected, because removal of protons from the system will lower the pH of the solution as it runs through the system. The calculated differences between the experimental and theoretical $[\text{OH}^-]$ decreased from 15 - 20 mM at the beginning to 5 - 6 mM at the end of the experiment. This smaller difference as the experiments proceeded was expected because the series of experiments began at the highest pH; the lines were conditioned more fully with each run. Although the difference in hydroxide concentrations is smallest at the end of the experiment, the discrepancy between theoretical and experimental pH values appears largest at the end of the experiment because pH is expressed on a log scale.

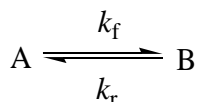
Figure 2.14 shows the experimental rates plotted against the theoretical hydroxide concentration as calculated from the serial dilution experiments. The straight line through the points gives a k_f of $161 \pm 8 \text{ M}^{-1} \text{ s}^{-1}$. The data points show some curvature, however, indicating that the pH values in the stopped-flow cell used during the experiment probably were not accurately known. This is also indicated by the y-intercept

of 1.29 ± 0.4 . This value for k_r is substantially greater than those calculated either from the y-intercept of the UV-visible experiments or those calculated from the forward rates of the UV-visible experiments and the equilibrium constants.

The bottom panel of Figure 2.14 shows the rates plotted as a function of the experimental hydroxide concentration as determined by the pH measurement of the solution after it had reacted and flowed through the lines to the output. It can be seen that the data points are not linear as a function of hydroxide concentration, indicating that this approach also did not give an accurate measurement of the hydroxide concentration in the stopped-flow cell during the experiment.

Figure 2.15 shows the same presentation for the second kinetic process. Fitting to a straight line gave a k_f of $5.0 \pm 0.1 \text{ M}^{-1} \text{ s}^{-1}$ and a k_r of $0.039 \pm 0.007 \text{ s}^{-1}$. The second kinetic process appears to give a slightly straighter line than the first, and to give a reasonable extrapolated value for k_r . However, this may be fortuitous. The hydroxide concentrations in the first and second kinetic processes are identical, as both reactions occurred in less than 10 s in the stopped-flow cell. As for the first reaction, plotting the data against the experimental concentrations of hydroxide produces a plot with significant curvature.

2.3.6 Calculating k_r . The reaction of the diimide to monoimide and monoimide to diamide are both reversible, as described above. Expressing this reversibility in general terms of A and B gives k_r as shown below:



$$K = \frac{k_f}{k_r}$$

$$K = \frac{[B]}{[A]}$$

$$\frac{k_f}{k_r} = \frac{[B]}{[A]}$$

$$k_r = k_f \frac{[A]}{[B]}$$

The fractions of species A and B at each pH were taken from the equilibria data (Figure 1.5). Table 2.5 shows k_r values calculated for the first process for **1**. The lower pH values (8.40 - 9.75) had an average k_r of $5.3 \pm 0.2 \times 10^{-4} \text{ s}^{-1}$. The stopped-flow pH values (11.8 - 13.0) had an average k_r of $9.0 \pm 1.7 \times 10^{-4} \text{ s}^{-1}$. Thus, these two values for k_r , calculated over approximately five orders of magnitude in $[\text{OH}^-]$, are within a factor of two of one another.

The k_r for the second process was $0.035 \pm 0.007 \text{ s}^{-1}$ using the formula above from the stopped-flow data. This was in agreement with experimental k_r of $0.039 \pm 0.007 \text{ s}^{-1}$ calculated by extrapolation of the stopped-flow data to the y axis in the plot of the rate as a function of $[\text{OH}^-]$.

2.3.7 Buffer contribution. To determine whether sodium tetraborate was catalyzing the reaction, the rate constant from the stopped-flow data at 0.1 M NaOH (161 s^{-1}) was used to calculate rate constants (k_{calc}) at much lower concentrations of hydroxide where the borate-buffered experiment had been run (k_{obs}). Table 2.6 shows that the k_{calc} and the k_{obs} rate constants are within 30% of each other. Therefore, borate does not act as a catalyst during hydrolysis.

2.3.8 The position of the charge in the side chain affects the rate of hydrolysis. This study shows that the distance of the cationic center from the central core affects the rates of hydrolysis: **1** hydrolyzes 6.8-fold faster than **5** (Figures 1.8 and 1.9). A similar effect of the position of the cationic group on the rate of the hydrolysis has also been seen in a study of the base-catalyzed hydrolysis of anilides.⁷³ Hydrolysis of an amide separated from a quaternary amine by a one-carbon linker [ArNHCOCH₂N⁺(CH₃)₃] or a three-carbon linker [ArNHCO(CH₂)₃N⁺(CH₃)₃] had rate constants of 4500 and 90 M⁻¹ h⁻¹, respectively.

2.4.0 Conclusions. Naphthalene diimides (NDIs) have a number of excellent characteristics that have led to their use in a variety of areas. First, they are excellent electron acceptors and have been used in this context in both photophysical and biophysical studies. Second, they are planar, but with side chains that can readily be created with charge. With cationic side chains, these planar species are excellent intercalators in nucleic acids, and they have been studied with a large number of different nucleic acid systems. The NDI core itself has double two-fold symmetry, which is retained if the side chains are identical. Changes in the side chains of these symmetrical NDI derivatives allow dissection of the factors which control intercalation in nucleic acid structures without the complications of more than one final intercalated structure. Derivatives with some water solubility are also increasingly used to make interesting three dimensional structures; the central cores can pack in various ways depending on the side chain substituents and other molecules in solution. Finally, the side chains can be elaborated to create additional functionality, e.g., metal centers. These are being used particularly in studies of the cleavage and analysis of nucleic acids.

A few years ago, the Dixon group showed that NDI derivatives with a cationic chain more than three atoms away from the central core would often at least partially self-stack in solution. This propensity to self-stack is valuable for some uses, but confuses quantitative nucleic acid binding studies. To create a new series of NDIs that would not self-stack, we synthesized derivatives with cationic charges two atoms away from the central core. We discovered that these molecules are quite sensitive to base. We investigated the base-catalyzed hydrolysis in some detail because, in view of the substantial current uses of water soluble NDIs, the basic chemistry of this system is of interest in many different contexts.

In this study, we have compared the hydrolysis and equilibria of NDI derivatives **1** and **5**, which have two or three methylene groups between the NDI core and the charge, respectively. The equilibrium constants, K_{a1} and K_{a2} , for the first and second hydrolyses of **1** were $2.5 \pm 0.2 \times 10^5 \text{ M}^{-1}$ and $2.0 \pm 0.1 \times 10^2 \text{ M}^{-1}$, respectively. The corresponding equilibrium constants for **5** were $1.4 \pm 0.1 \times 10^5 \text{ M}^{-1}$ and $44 \pm 2 \text{ M}^{-1}$, respectively. The rate of the first hydrolysis of NDI **1** was 7-fold faster than that of NDI **5**. At physiological pH (7.4), the half-life for **1** was 37 h while the half-life for **5** was 241 h. Our data would indicate that NDIs with side chains that have a cationic charge separated from the central core by three carbon atoms are considerably more stable toward hydrolysis by base than derivatives with the cationic charge two atoms away from the central core.

Table 2.1. Chemical shifts of the geometric isomers of the diamide form of **1** in D₂O at selected temperatures. Only the two inner peaks of the AB-quartet are reported for the *anti* isomer

Temperature (°C)	<i>syn</i> (, ppm)	<i>syn</i> (, ppm)	<i>anti</i> (, ppm)	<i>anti</i> (, ppm)
30	7.39	7.43	7.41	7.40
50	7.77	7.82	7.78	7.80
70	7.73	7.78	7.73	7.76

Table 2.2. The *k_f* and *k_r* of NDIs **1** and **5**. UV-visible experiments were performed in 100 mM borate buffer; the stopped-flow experiment was run without buffer. The *k_f* and the *k_r* are derived from the slopes and the intercepts, respectively, of the rates as a function of [OH⁻]

Experiment		<i>k_f</i> , M ⁻¹ s ⁻¹	<i>k_r</i> , s ⁻¹
UV-visible	1	130 ± 3	0.11 ± 7.6 x 10 ⁻⁵
UV-visible	5	20 ± 0.3	0.039 ± 1.2 x 10 ⁻⁵
Stopped flow	1 , <i>k_{obs1}</i>	161 ± 8	1.29 ± 0.41
Stopped flow	1 , <i>k_{obs2}</i>	5.0 ± 0.1	0.039 ± 0.007

Table 2.3. Average k_{obs} for both processes at each concentration of NaOH (calculated using serial dilutions) from the stopped-flow data

[NaOH], mM	$k_{\text{obs1}}, \text{s}^{-1}$	$k_{\text{obs2}}, \text{s}^{-1}$
100	17.0 ± 0.2	$53.0 \pm 0.1 \times 10^{-2}$
50	9.94 ± 0.10	$30.0 \pm 0.2 \times 10^{-2}$
25	5.82 ± 0.02	$17.0 \pm 0.1 \times 10^{-2}$
12.5	3.20 ± 0.03	$10.0 \pm 0.01 \times 10^{-2}$
6.25	1.69 ± 0.01	$60.0 \pm 0.3 \times 10^{-3}$

Table 2.4. The theoretical and experimental concentrations of NaOH and the difference between them

[NaOH], mM	Theoretical pH	Experimental [NaOH], mM	Experimental pH	mM
100	13.0	115	13.06	15.0
50	12.7	30.2	12.48	19.8
25	12.4	11.8	12.07	13.2
12.5	12.1	2.88	11.46	9.62
6.25	11.8	0.62	10.79	5.63

Table 2.5. Calculated k_r using fractions of HA and A^- from equilibrium data

Sodium Tetraborate Buffer	pH calc	Fraction of HA	Fraction of A^-	k_{obs}, s^{-1}	k_r calc, s^{-1}
	8.40	6.09×10^{-1}	0.391	3.55×10^{-4}	5.52×10^{-4}
	8.71	4.38×10^{-1}	0.561	6.47×10^{-4}	5.04×10^{-4}
	9.31	1.63×10^{-1}	0.833	2.73×10^{-3}	5.35×10^{-4}
	9.51	1.12×10^{-1}	0.883	4.04×10^{-3}	5.11×10^{-4}
	9.75	6.57×10^{-2}	0.924	7.34×10^{-3}	5.22×10^{-4}
Stopped- Flow	pH calc	Fraction of HA	Fraction of A^-	k_{obs}, s^{-1}	k_r calc, s^{-1}
	11.80	2.80×10^{-4}	4.42×10^{-1}	1.69	1.07×10^{-3}
	12.10	9.39×10^{-5}	2.89×10^{-1}	3.20	1.04×10^{-3}
	12.40	2.64×10^{-5}	1.66×10^{-1}	5.82	9.26×10^{-4}
	12.70	7.24×10^{-6}	9.07×10^{-2}	9.94	7.93×10^{-4}
	13.00	1.90×10^{-6}	4.76×10^{-2}	17.0	6.81×10^{-4}

Table 2.6. Using $k = 161 M^{-1}s^{-1}$ (from stopped-flow data) to find k_{calc} (see text)

pH	$OH^- (M^{-1})$	$k_{obs}, M^{-1}s^{-1}$	$k_{calc}, M^{-1}s^{-1}$	k_{calc}/k_{obs}
8.40	2.51×10^{-6}	3.55×10^{-4}	4.05×10^{-4}	1.14
8.71	5.13×10^{-6}	6.47×10^{-4}	8.27×10^{-4}	1.28
9.31	2.04×10^{-5}	2.73×10^{-3}	3.29×10^{-3}	1.20
9.51	3.24×10^{-5}	4.04×10^{-3}	5.22×10^{-3}	1.29
9.75	5.62×10^{-5}	7.34×10^{-3}	9.07×10^{-3}	1.23

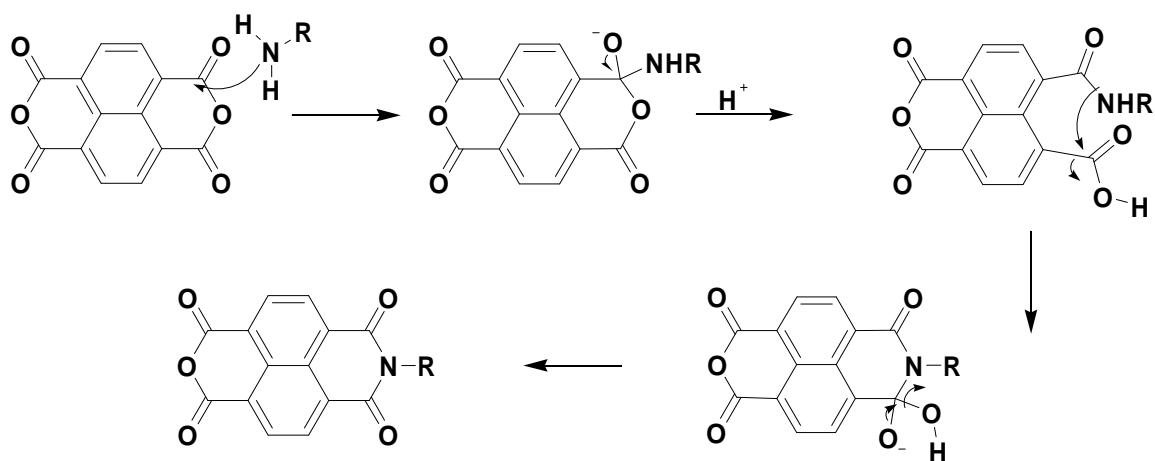


Figure 2.1. Proposed mechanism for the synthesis of the imide ring.

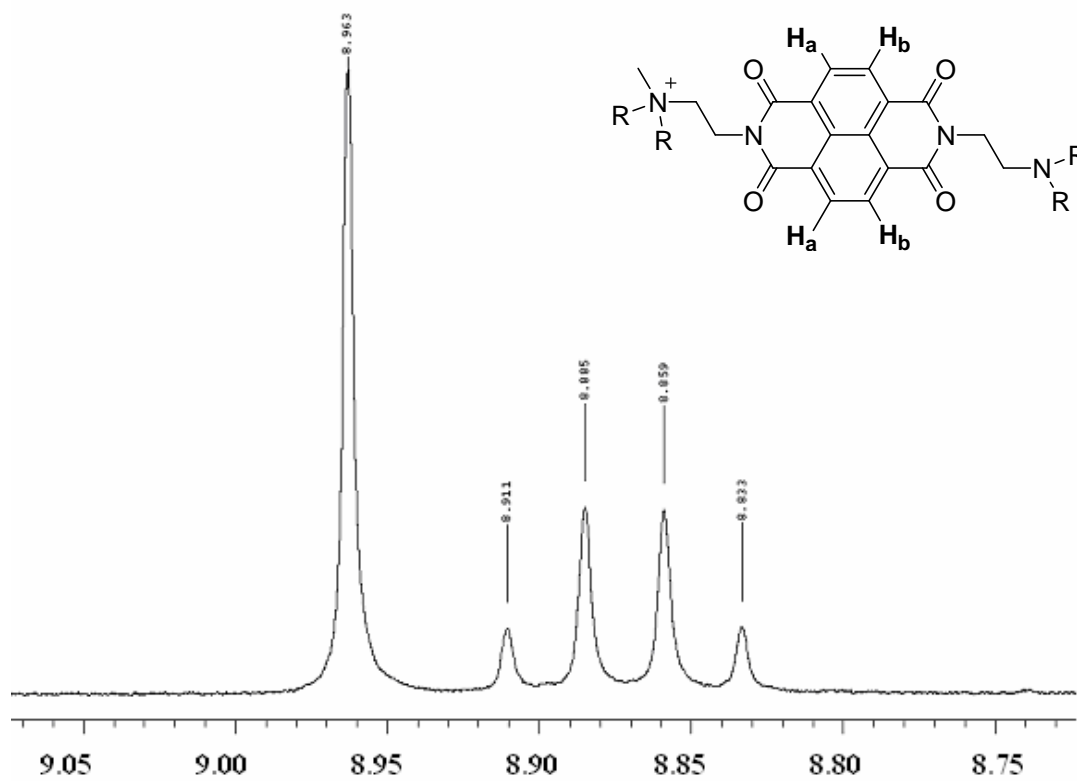


Figure 2.2. NMR spectrum of monoalkylated **4** in D₂O. The inset shows the structure with the aromatic protons labeled.

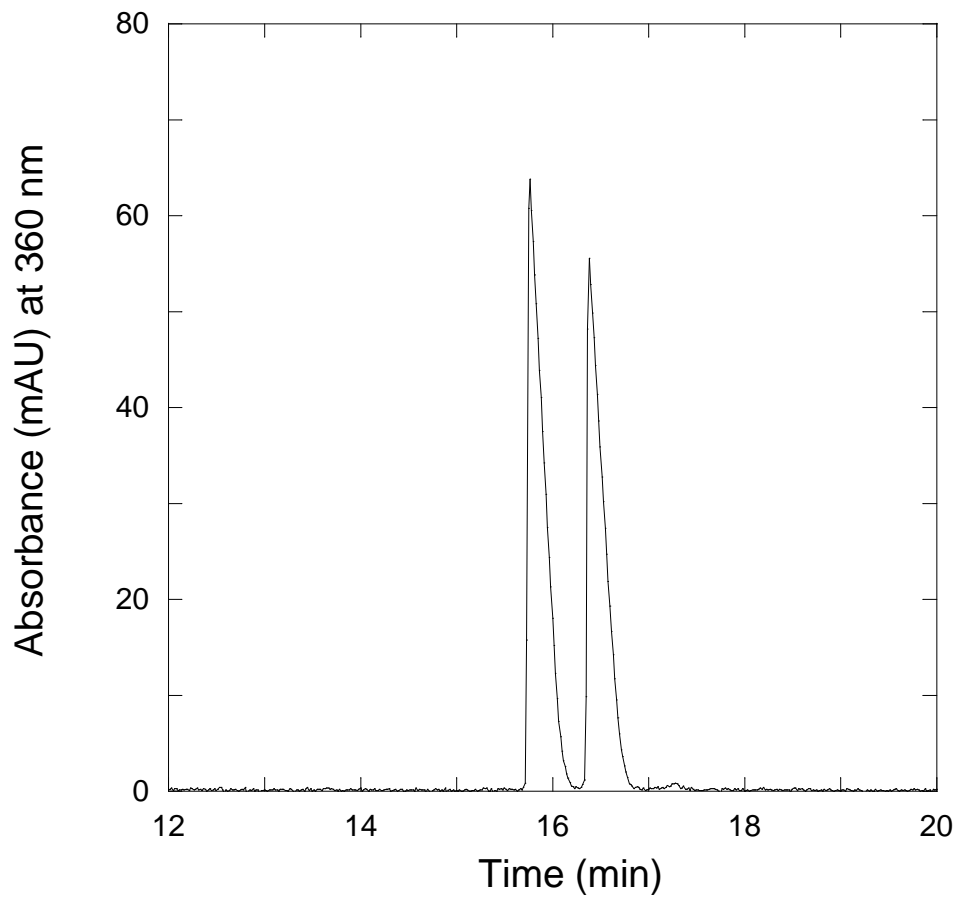


Figure 2.3. Electropherogram of **4** and its monoalkylated precursor, 50 mM sodium phosphate buffer, pH 3.0, 11 kV.

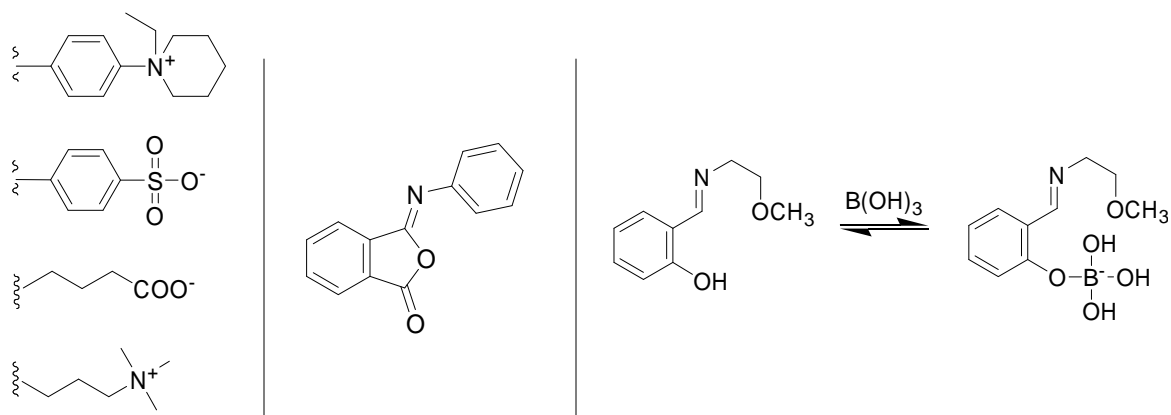


Figure 2.4. (Left) Side chains of aromatic NDIs discussed in the text. (Center) Structure of the isoimide investigated by Ernst and Schmir (see text). (Right) Proposed intermediate in which borate acts as an intramolecular catalyst.

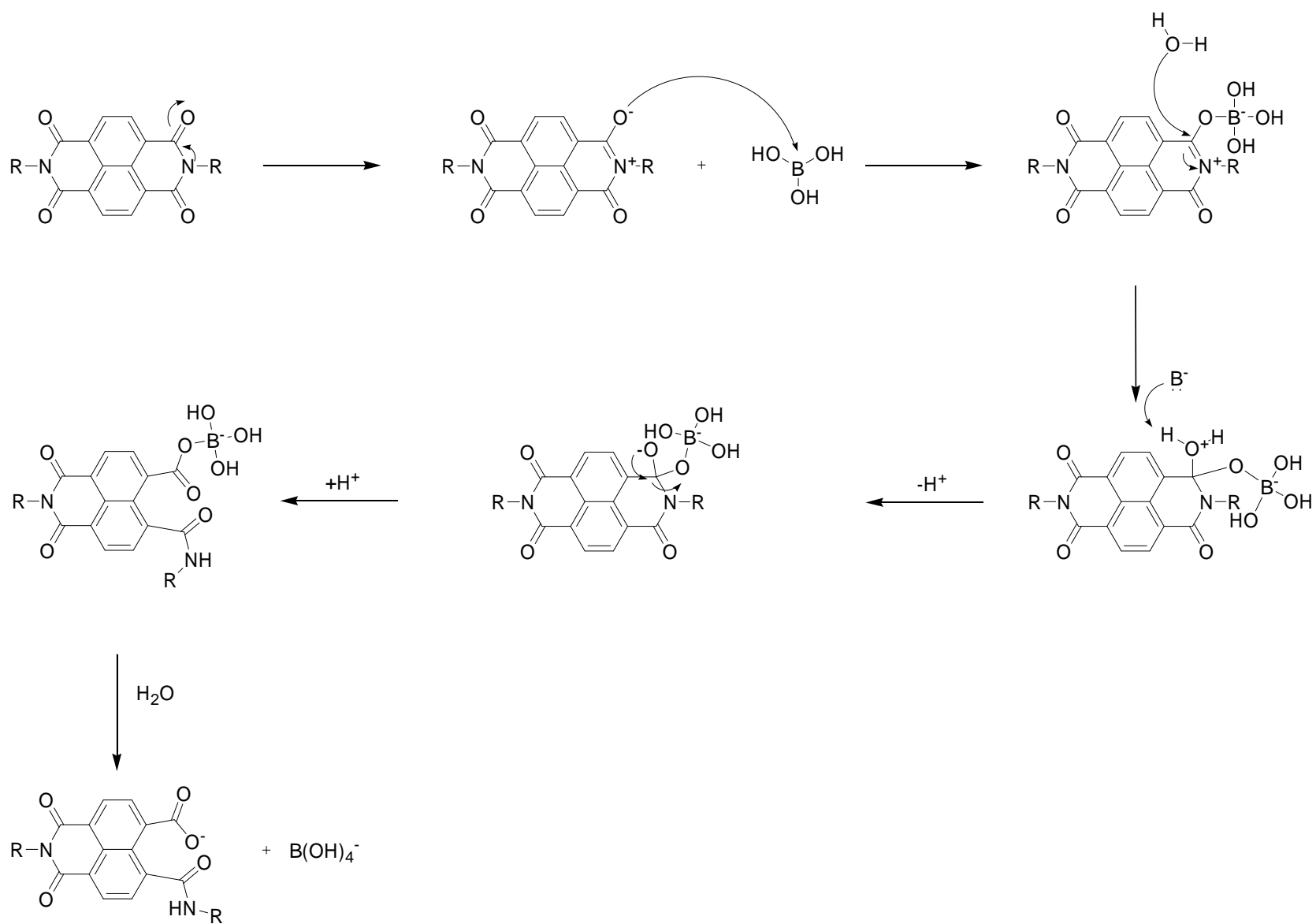


Figure 2.5. Proposed mechanism for the hydrolysis of the imide ring with borate as a nucleophilic catalyst.

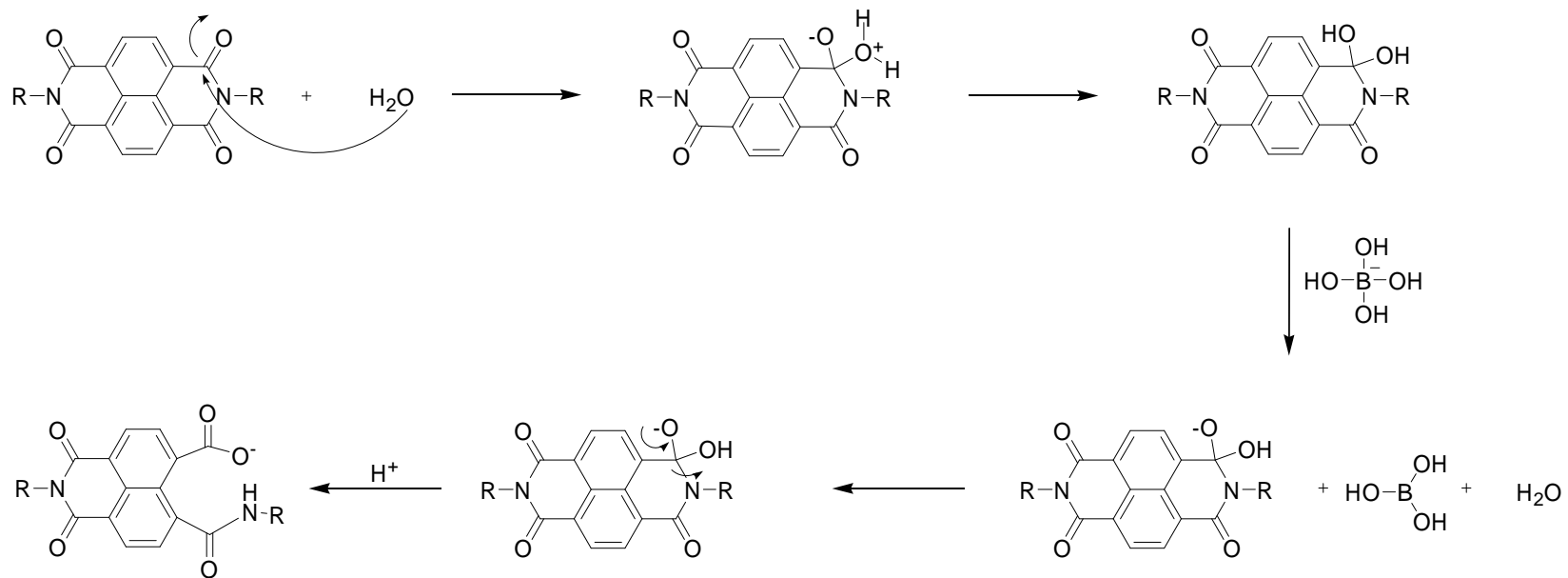


Figure 2.6. Proposed mechanism for the hydrolysis of the imide ring with borate as a general base.

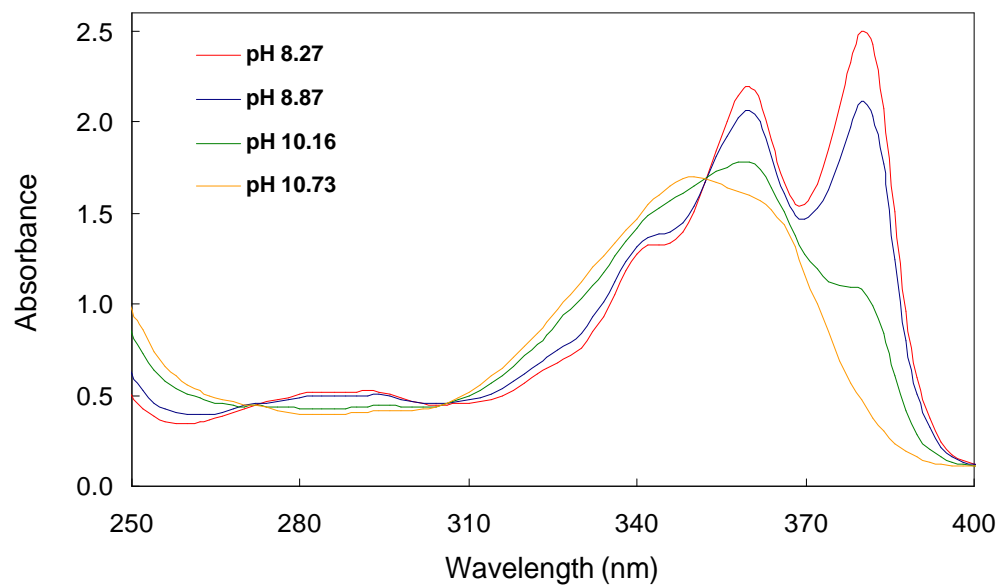


Figure 2.7. Absorbance of a solution of **1** as a function of pH. The reaction was run in 50 mM sodium phosphate buffer by adding aliquots of 0.1 M NaOH.

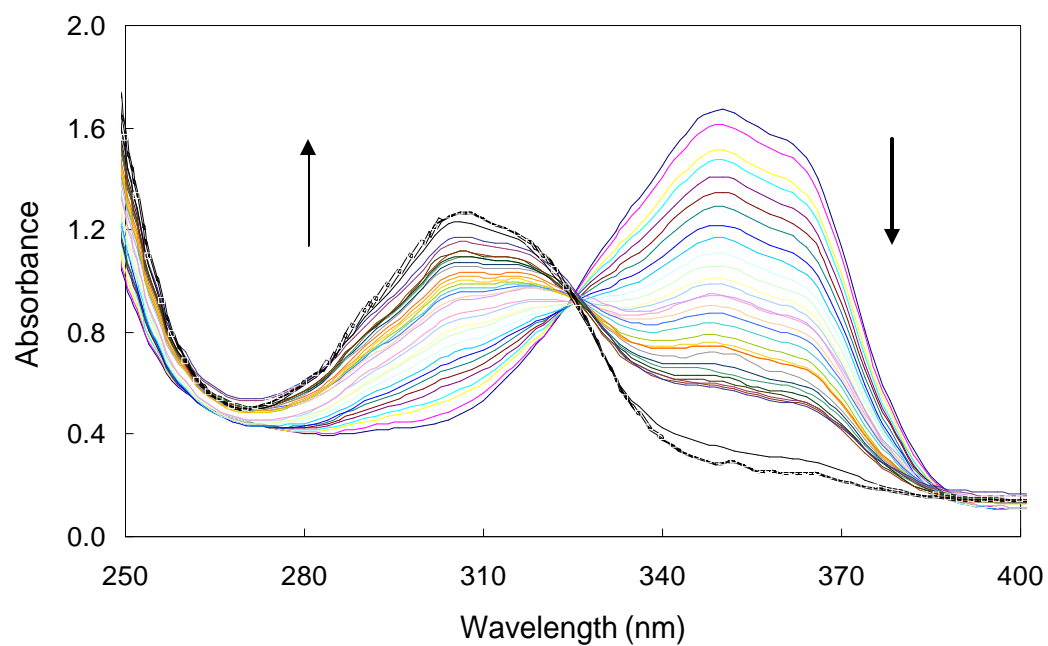


Figure 2.8. Absorbance a solution of **1** as a function of pH. The reaction was run in 50 mM sodium phosphate buffer by adding aliquots of 0.1 M NaOH.

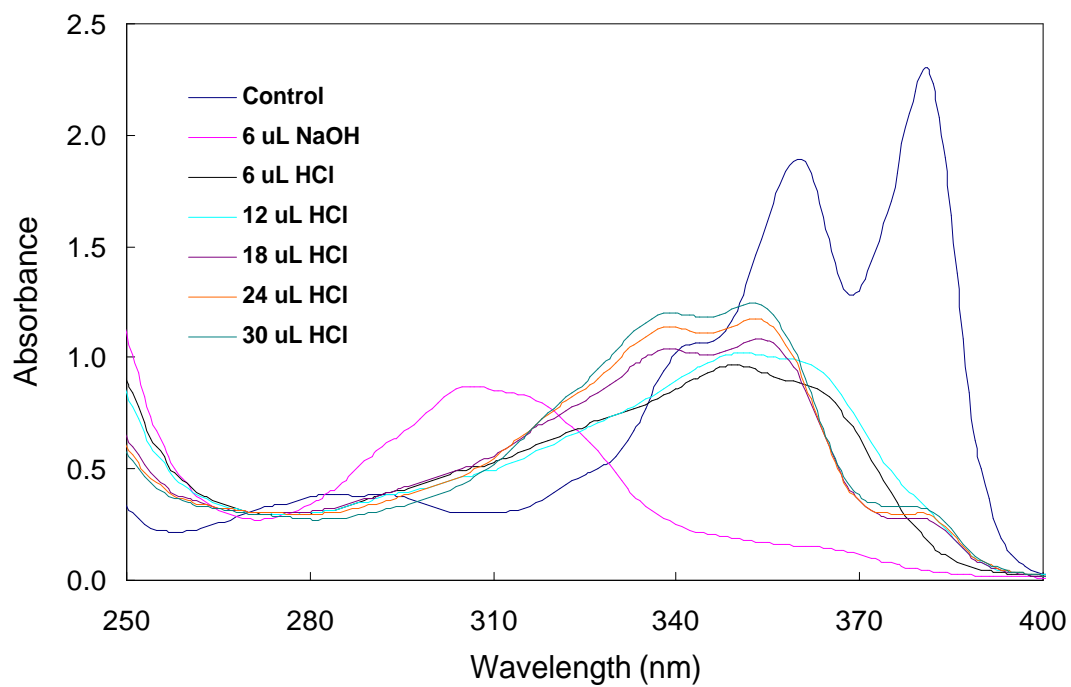


Figure 2.9. UV-visible spectra following the attempted ring closure of **1** in 50 mM sodium phosphate buffer by addition of aliquots of 12 M HCl.

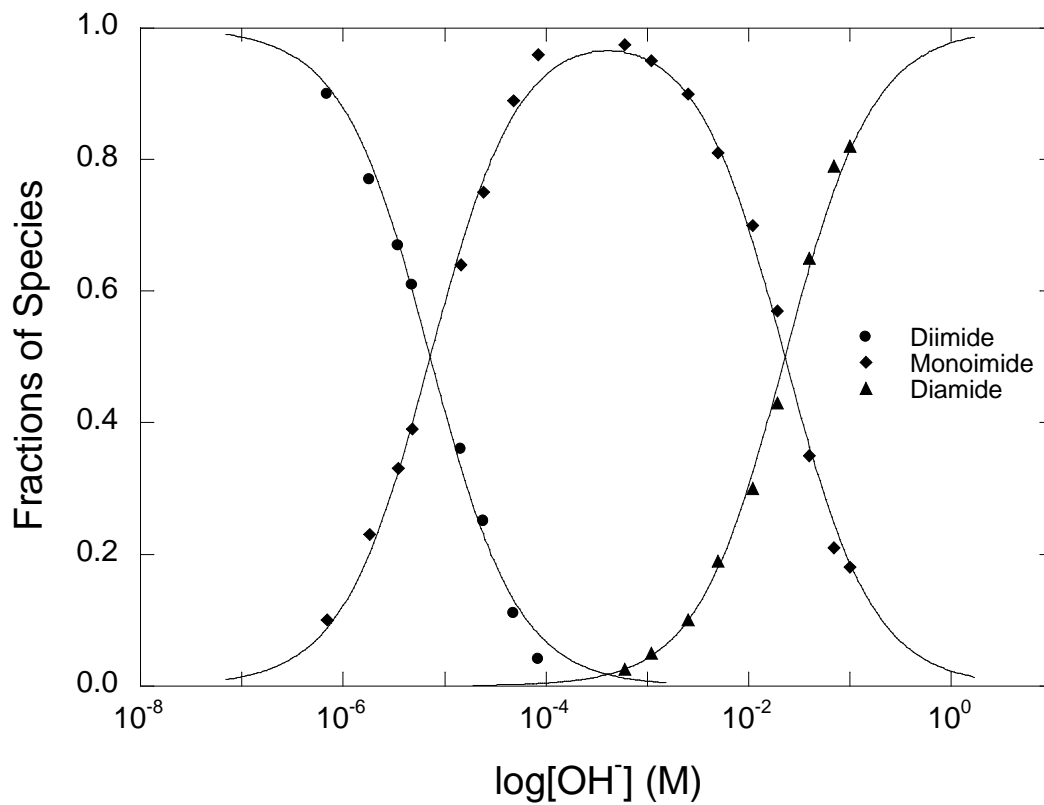


Figure 2.10. Fractions of the diimide, monoimide and diamide as a function of pH. Samples of **5** were equilibrated in a buffer containing 100 mM sodium phosphate and 100 mM sodium tetraborate.

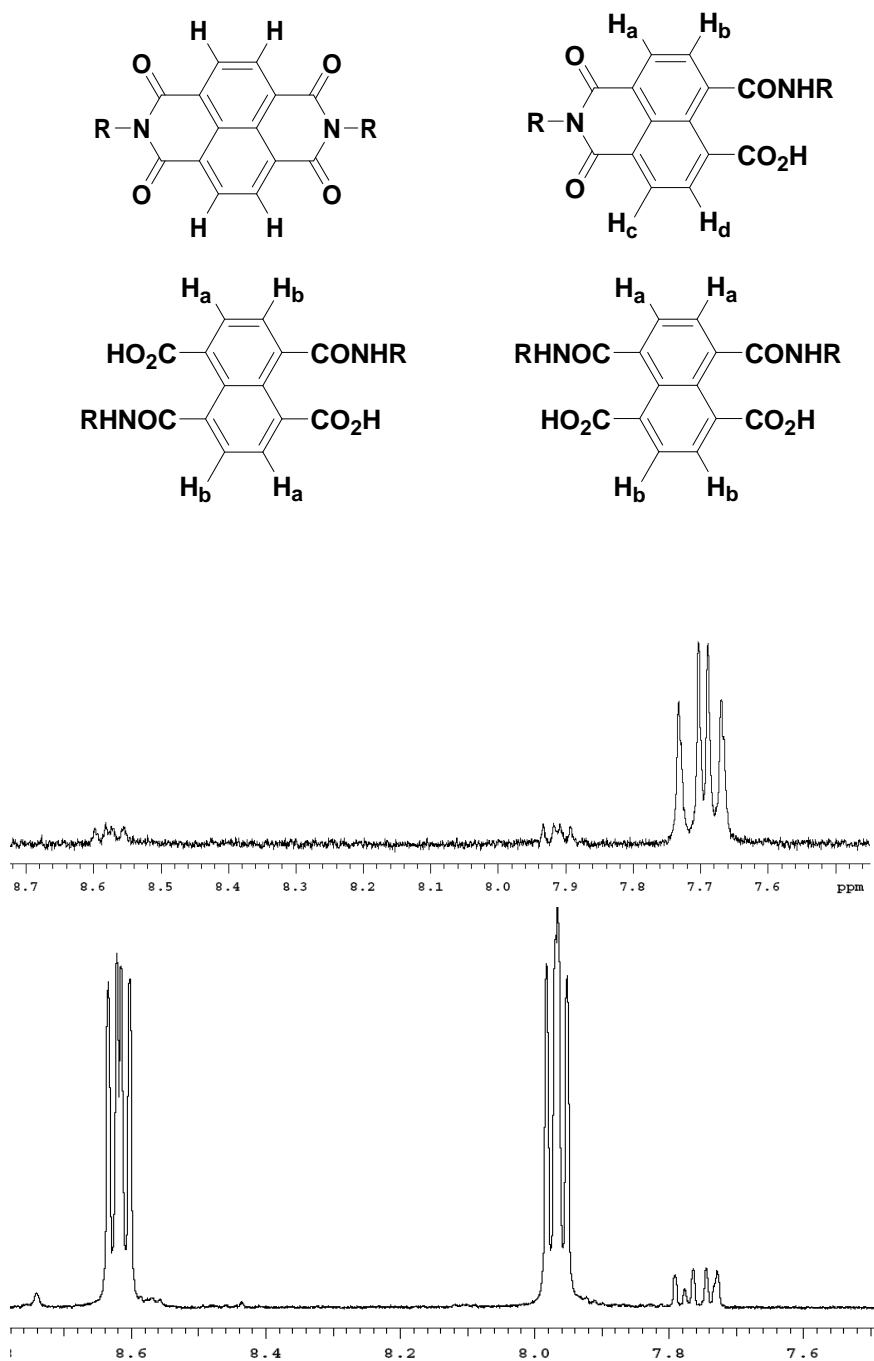


Figure 2.11. (Top) Designation of the aromatic protons on the NDI in the hydrolysis products. (Middle) ¹H 300 MHz NMR spectrum of **1** in D₂O with the addition of NaOD. (Bottom) ¹H 600 MHz NMR spectrum of **1** in D₂O after five days.

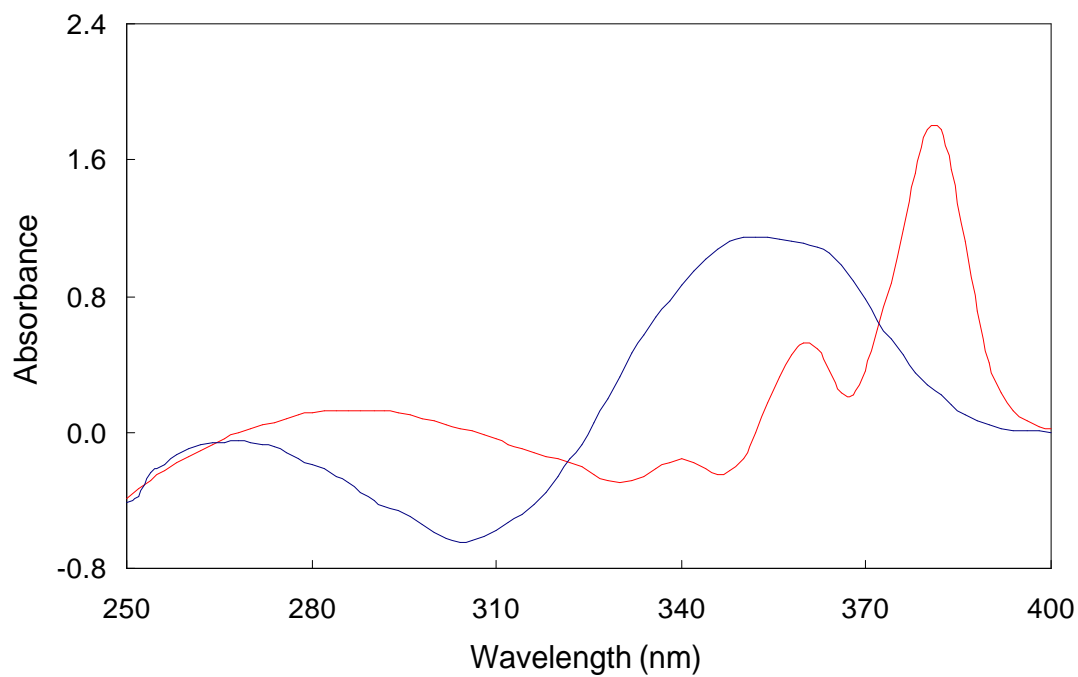


Figure 2.12. Difference spectra of the UV-visible absorbances for the three species of **1**. Difference spectra of the UV-visible absorbances for the diimide-monoimide (maximum at 380 nm) and monoimide-diamide (broad peak from 340 nm to 370 nm). The lines intersect at 372 nm, where the changes in absorbance between the species are the same.

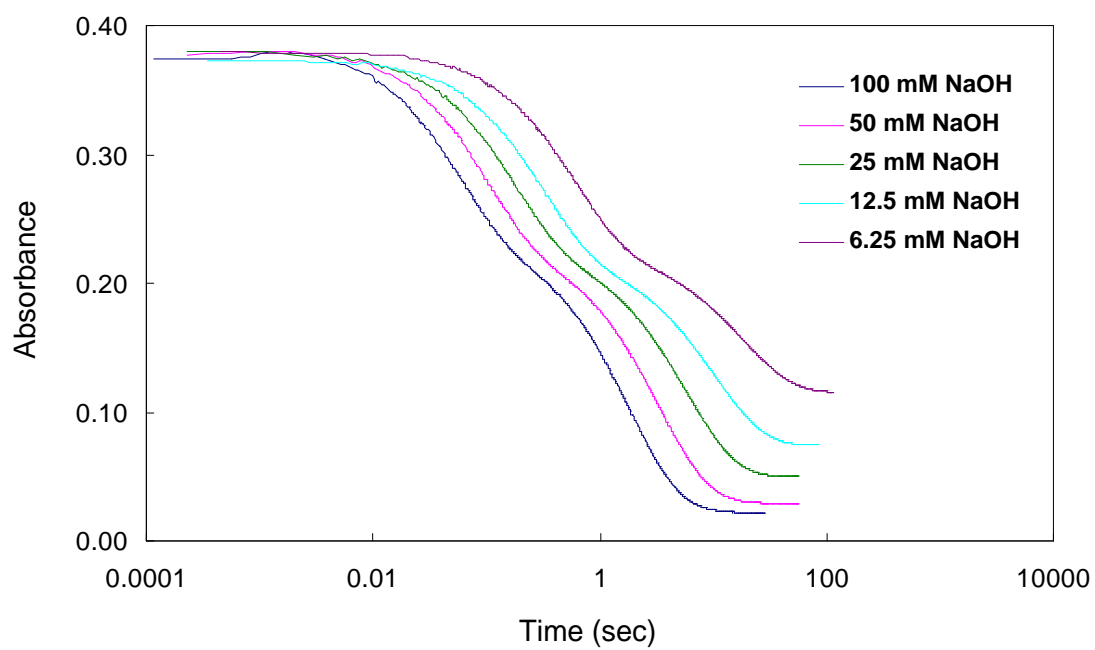


Figure 2.13. Absorbance as a function of time for **1** in the presence of different concentrations of NaOH.

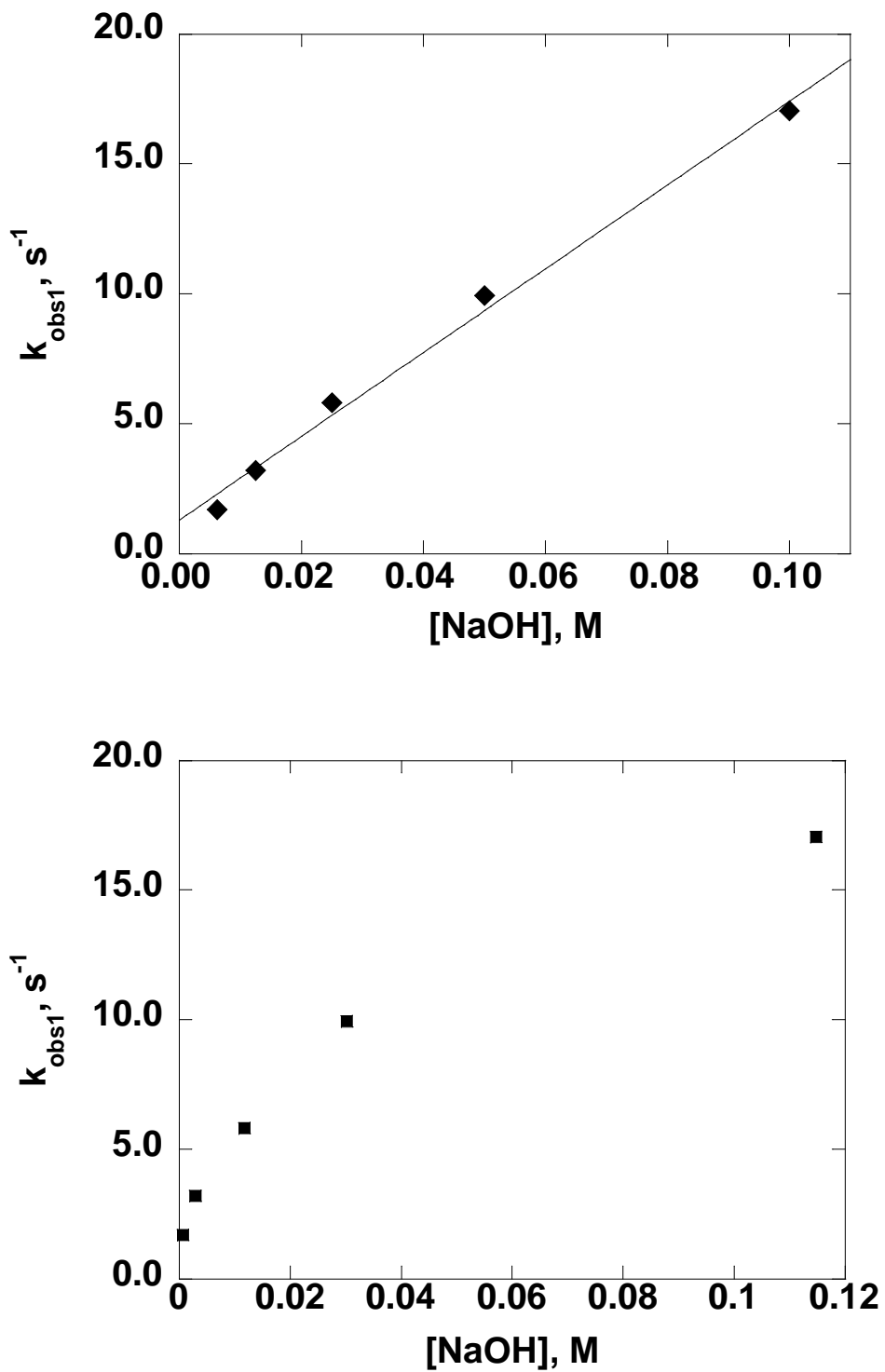


Figure 2.14. (Top) Rate of the first hydrolysis of **1** as a function of $[\text{OH}^-]$ calculated via serial dilution. (Bottom) Rate of the first hydrolysis of **1** as a function of $[\text{OH}^-]$ measured experimentally after completion of the reaction at the output of the system.

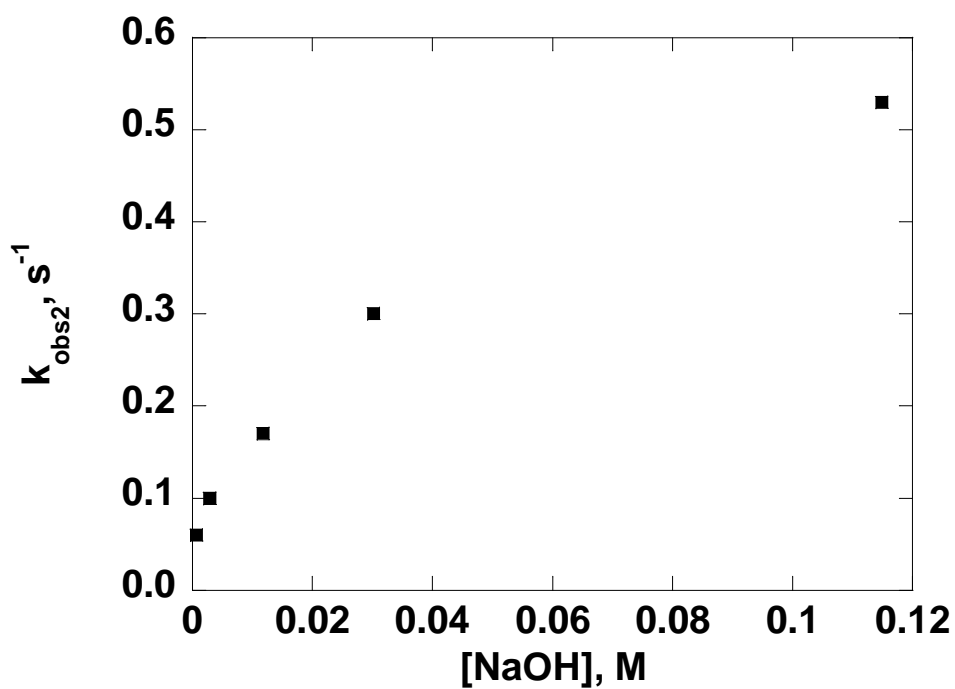
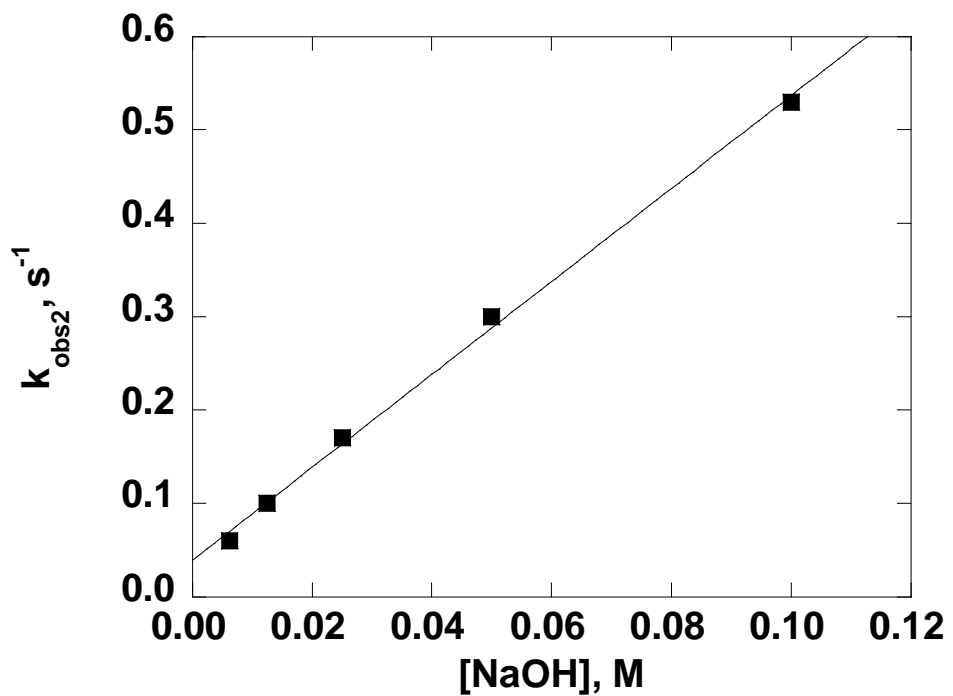


Figure 2.15. (Top) Rate of the second hydrolysis of **1** as a function of $[\text{OH}^-]$ calculated via serial dilution. (Bottom) Rate of the second hydrolysis of **1** as a function of $[\text{OH}^-]$ measured experimentally after completion of the reaction at the output of the system.

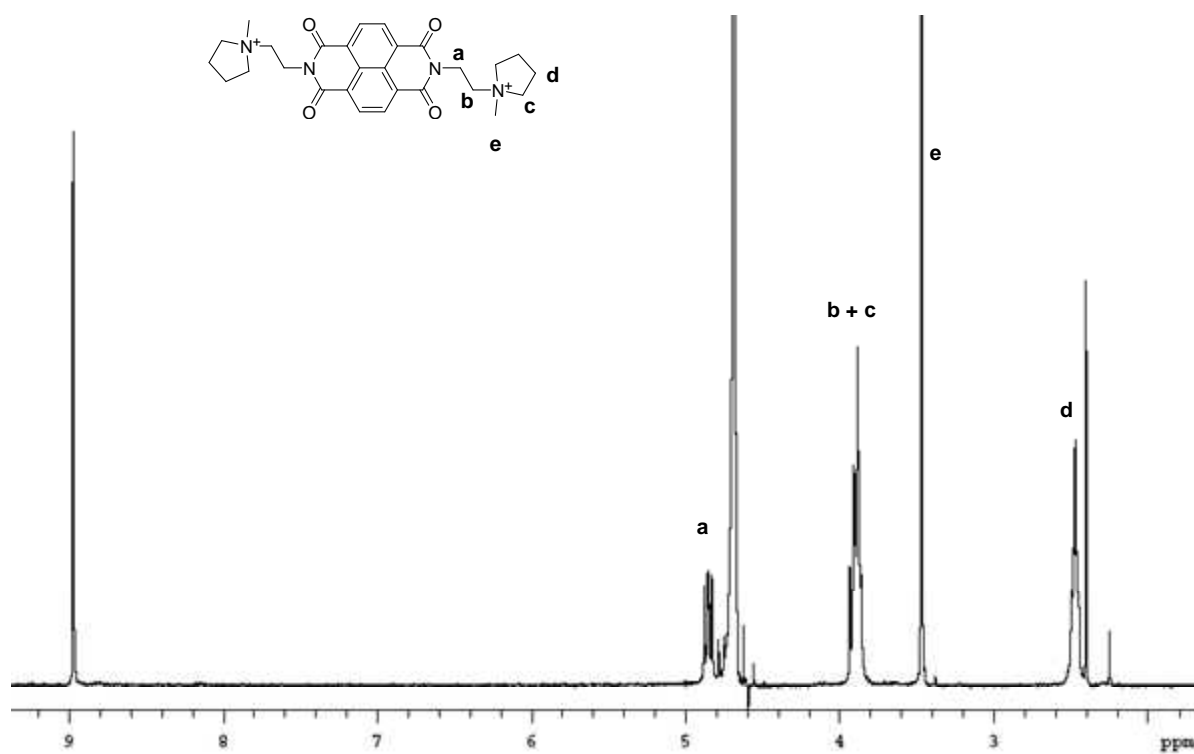


Figure 2.16. ^1H NMR spectrum of **1** at 300 MHz in D_2O .

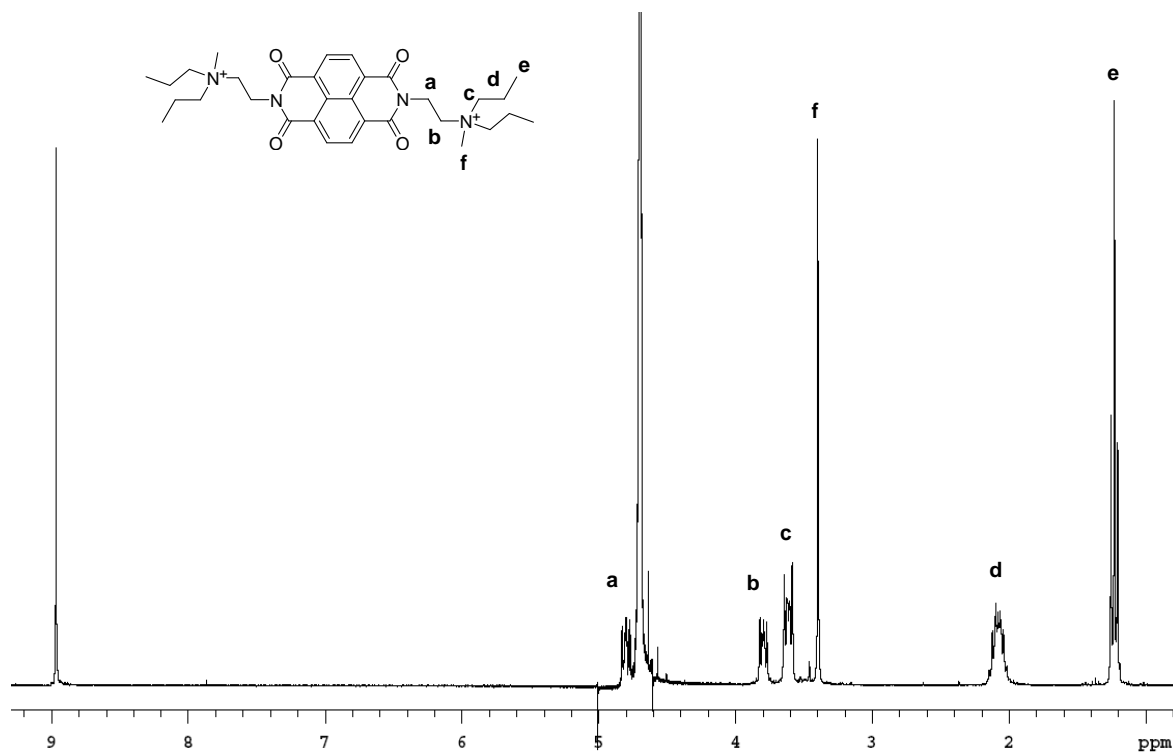


Figure 2.17. ^1H NMR spectrum of **2** at 300 MHz in D_2O .

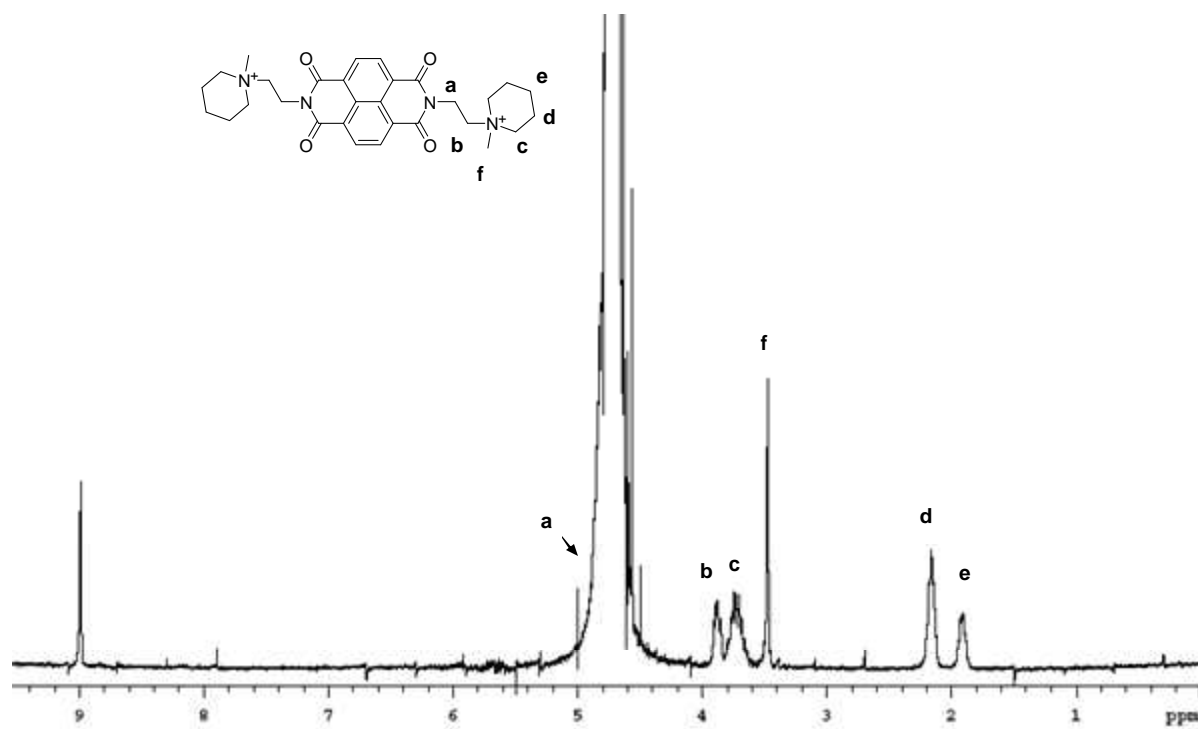


Figure 2.18. ^1H NMR spectrum of **3** at 300 MHz in D_2O .

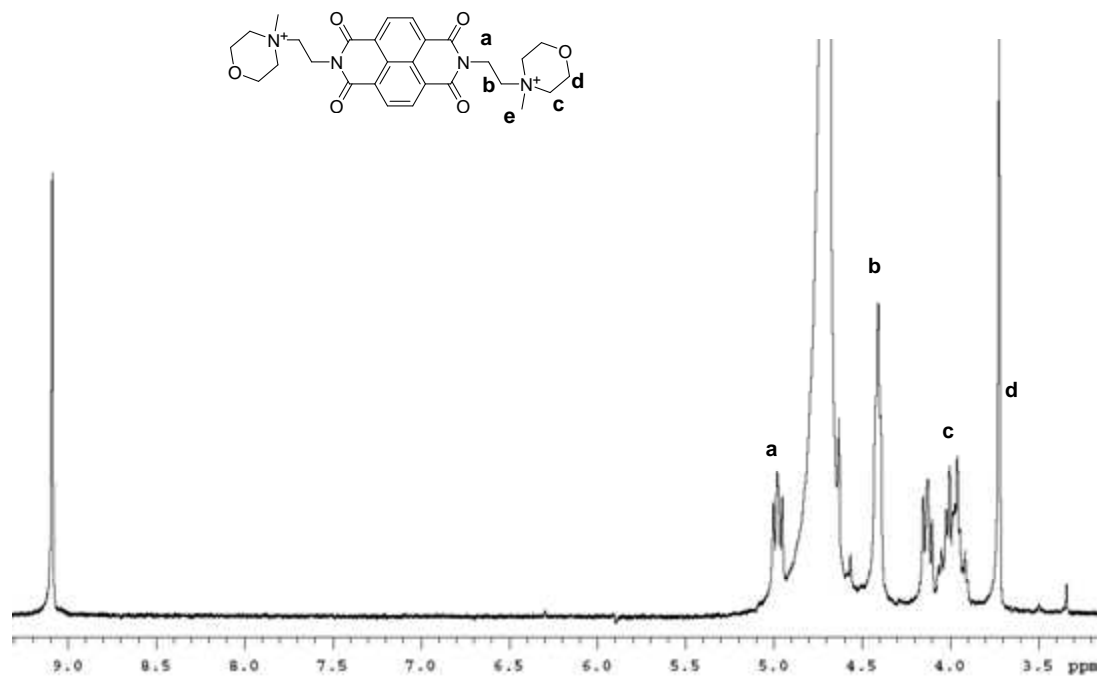


Figure 2.19. ^1H NMR spectrum of **4** at 300 MHz in D_2O .

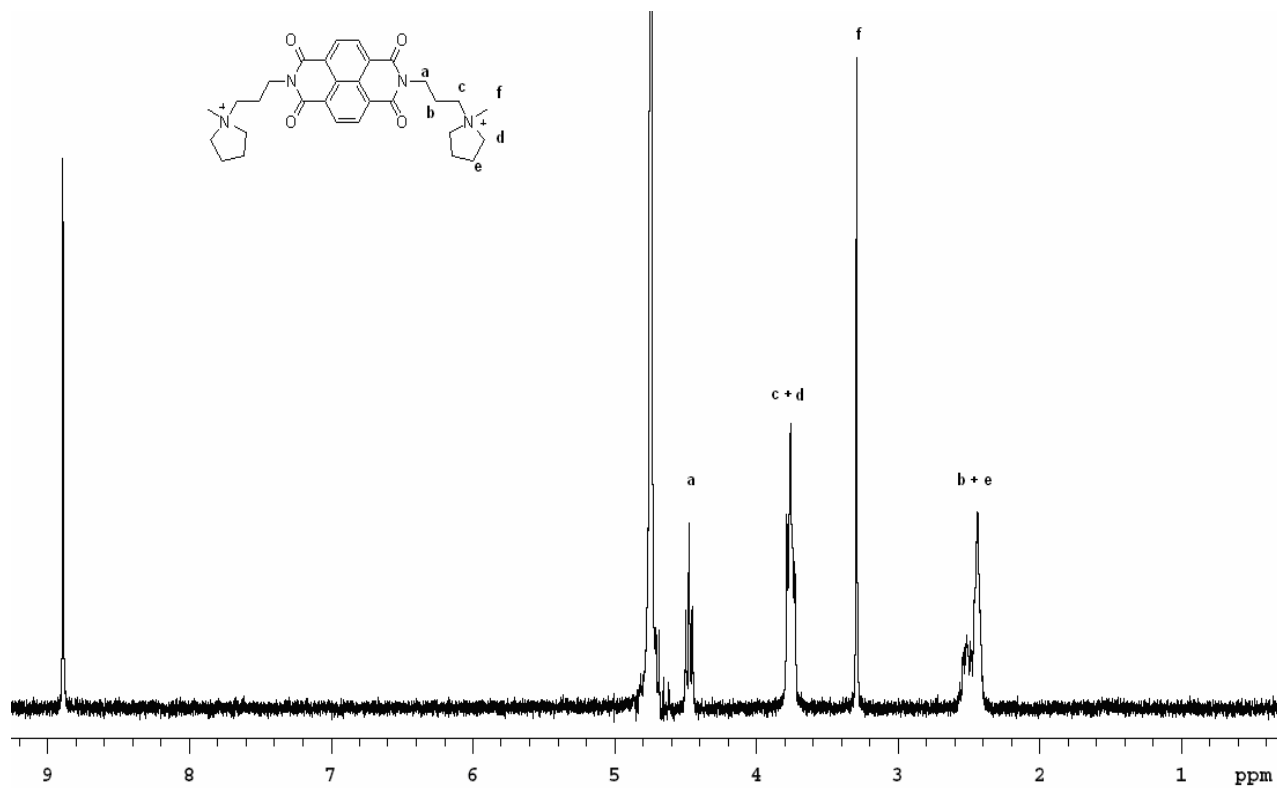


Figure 2.20. ^1H NMR spectrum of **5** at 300 MHz in D_2O .

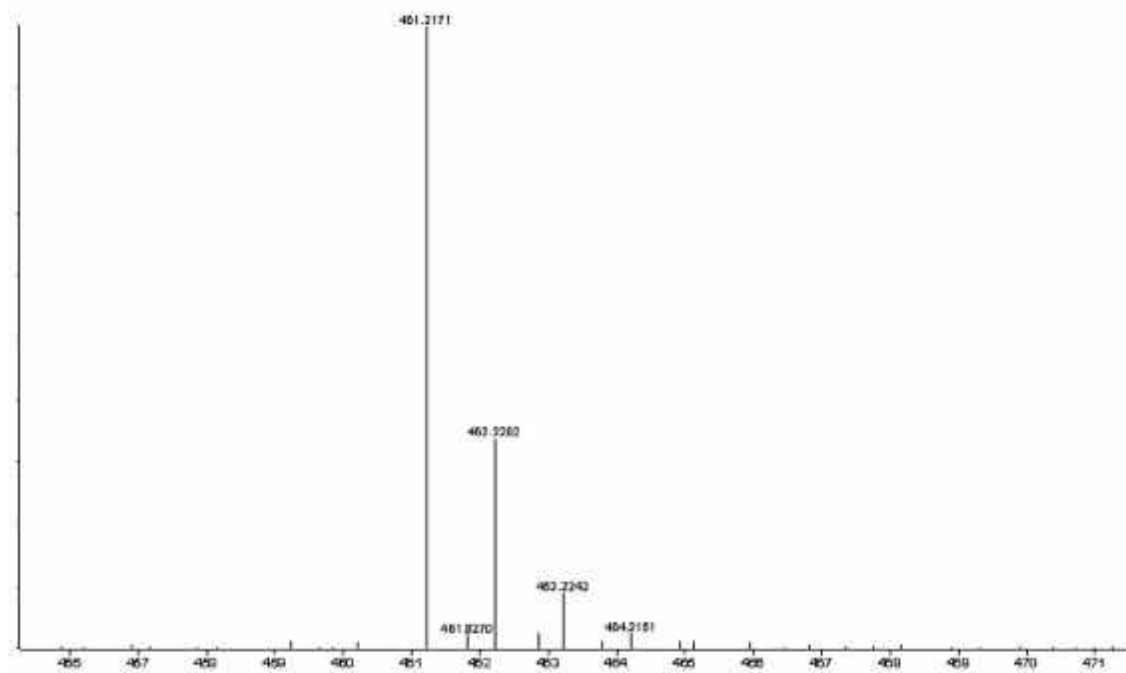


Figure 2.21. Electrospray (ESI) high resolution mass spectrum from positive ion mode of NDI **1**. The exact mass is 461.2171 m/z.

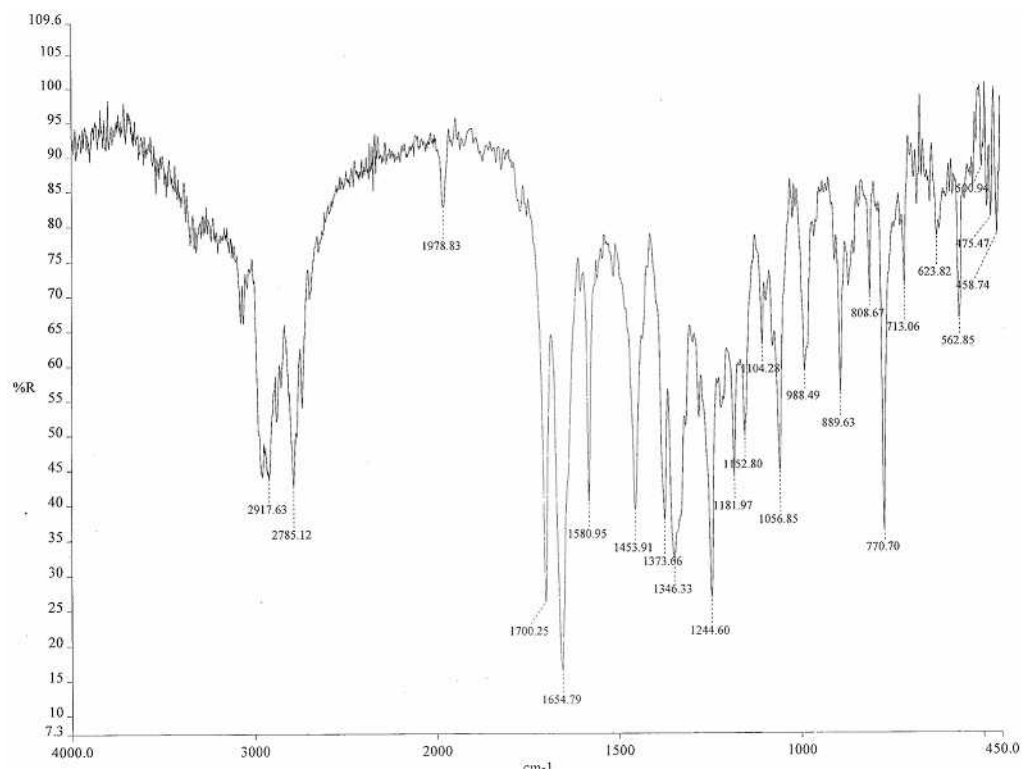


Figure 2.22. Infrared spectrum of **1**.

Reference List

1. Miller LL, Mann KR. *Acc. Chem. Res.*, π -Dimers and π -stacks in solution and in conducting polymers, 1996; **29**: 417-423.
2. Miller LL, Duan RG, Tully DC, Tomalia DA. *J. Am. Chem. Soc.*, Electrically conducting dendrimers, 1997; **119**: 1005-1010.
3. Zhao XY, Pinto MR, Hardison LM, Mwaura J, Muller J, Jiang H, Witker D, Kleiman VD, Reynolds JR, Schanze KS. *Macromolecules*, Variable band gap poly(arylene ethynylene) conjugated polyelectrolytes, 2006; **39**: 6355-6366.
4. Aveline BM, Matsugo S, Redmond RW. *J. Am. Chem. Soc.*, Photochemical mechanisms responsible for the versatile application of naphthalimides and naphthalidiimides in biological systems, 1997; **119**: 11785-11795.
5. Barros TC, Brochsztain S, Toscano VG, Berci P, Politi MJ. *J. Photochem. Photobiol. A*, Photophysical characterization of a 1,4,5,8-naphthalenediimide derivative, 1997; **111**: 97-104.
6. Rogers JE, Kelly LA. *J. Am. Chem. Soc.*, Nucleic acid oxidation mediated by naphthalene and benzophenone imide and diimide derivatives: Consequences for DNA redox chemistry, 1999; **121**: 3854-3861.
7. Rodrigues MA, Brochsztain S, Barros TC, Baptista MS, Politi MJ. *Photochem. Photobiol.*, pH-dependent excited-state properties of *N,N'*-di(2-phosphonoethyl)-1,4,5,8-naphthalenediimide, 1999; **70**: 35-39.

8. Rogers JE, Weiss SJ, Kelly LA. *J. Am. Chem. Soc.*, Photoprocesses of naphthalene imide and diimide derivatives in aqueous solutions of DNA, 2000; **122**: 427-436.
9. Abraham B, McMasters S, Mullan MA, Kelly LA. *J. Am. Chem. Soc.*, Reactivities of carboxyalkyl-substituted 1,4,5,8-naphthalene diimides in aqueous solution, 2004; **126**: 4293-4300.
10. Figueiredo KM, Marcon RO, Campos IB, Nantes IL, Brochsztain S. *J. Photochem. Photobiol. B*, Photoinduced electron transfer between cytochrome c and a novel 1,4,5,8-naphthalenetetracarboxylic diimide with amphiphilic character, 2005; **79**: 1-9.
11. Matsugo S, Yan LJ, Han D, Packer L. *Biochem. Biophys. Res. Commun.*, Induction of protein oxidation in human low lipoprotein by the photosensitive organic hydroperoxide, *N,N'*-bis(2-hydroxyperoxy-2-methoxyethyl)-1,4,5,8-naphthalene tetracarboxylic diimide, 1995; **206**: 138-145.
12. Campos IB, Nantes IL, Politi MJ, Brochsztain S. *Photochem. Photobiol.*, Photochemical reduction of cytochrome c by a 1,4,5,8-naphthalenediimide radical anion, 2004; **80**: 518-524.
13. Matsugo S, Kawanishi S, Yamamoto K, Sugiyama H, Matsuura T, Saito I. *Angew. Chem. Int. Ed.*, Bis(hydroperoxy)naphthaldiimide as a photo-Fenton reagent - sequence-specific photocleavage of DNA, 1991; **30**: 1351-1353.

14. Matsugo S, Kodaira K, Saito I. *Bioorg. Med. Chem. Lett.*, Transfecting activity of photoirradiated Phi-X 174 DNA in the presence of hydroperoxynaphthalimides, 1993; **3**: 1671-1674.
15. Nakajima M, Takeuchi T, Ogino K, Morimoto K. *Jpn. J. Cancer Res.*, Lack of direct involvement of 8-hydroxy-2'-deoxyguanosine in hypoxanthineguanine phosphoribosyltransferase mutagenesis in V79 cells treated with *N,N'*-bis(2-hydroxyperoxy-2-methoxyethyl)-1,4,5,8-naphthalenetetracarboxylic-diimide (NP-III) or riboflavin, 2002; **93**: 247-252.
16. Tomasulo M, Naistat DM, White AJP, Williams DJ, Raymo FM. *Tetrahedron Lett.*, Self-assembly of naphthalene diimides into cylindrical microstructures, 2005; **46**: 5695-5698.
17. Zych AJ, Iverson BL. *Helv. Chim. Acta*, Conformational modularity of an abiotic secondary-structure motif in aqueous solution, 2002; **85**: 3294-3300.
18. Gabriel GJ, Sorey S, Iverson BL. *J. Am. Chem. Soc.*, Altering the folding patterns of naphthyl trimers, 2005; **127**: 2637-2640.
19. Gabbay EJ, DeStefano R, Baxter CS. *Biochem. Biophys. Res. Commun.*, Topography of nucleic helices in solutions. XXVIII. Evidence for a dynamic structure of DNA in solution, 1973; **51**: 1083.
20. Yen S-F, Gabbay EJ, Wilson WD. *Biochemistry*, Interaction of aromatic imides with deoxyribonucleic acid. Spectrophotometric and viscometric studies, 1982; **21**: 2070-2076.

21. Tanious FA, Yen S-F, Wilson WD. *Biochemistry*, Kinetic and equilibrium analysis of a threading intercalation mode: DNA sequence and ion effects, 1991; **30**: 1813-1819.
22. Takenaka S, Yokoyama M, Kondo H. *Chem. Commun.*, Selective stabilization of a bulged duplex of d(GCGAACGC) oligonucleotide by thymine base-substituted naphthalene diimide, 1997; 115-116.
23. Bevers S, Schutte S, McLaughlin LW. *J. Am. Chem. Soc.*, Naphthalene- and perylene-based linkers for the stabilization of hairpin triplexes, 2000; **122**: 5905-5915.
24. Gianolio DA, McLaughlin LW. *Bioorg. Med. Chem.*, Tethered naphthalene diimide intercalators enhance DNA triplex stability, 2001; **9**: 2329-2334.
25. Fedoroff OY, Salazar M, Han HY, Chemeris VV, Kerwin SM, Hurley LH. *Biochemistry*, NMR-based model of a telomerase-inhibiting compound bound to G-quadruplex DNA, 1998; **37**: 12367-12374.
26. Han HY, Bennett RJ, Hurley LH. *Biochemistry*, Inhibition of unwinding of G-quadruplex structures by Sgs1 helicase in the presence of *N,N'*-bis[2-(1-piperidino)ethyl]-3,4,9,10-perylenetetracarboxylic diimide, a G-quadruplex-interactive ligand, 2000; **39**: 9311-9316.
27. Sato S, Kondo H, Nojima T, Takenaka S. *Anal. Chem.*, Electrochemical telomerase assay with ferrocenyl naphthalene diimide as a tetraplex DNA-specific binder, 2005; **77**: 7304-7309.

28. Sato S, Fujii S, Yamashita K, Takagi M, Kondo H, Takenaka S. *J. Organometal. Chem.*, Ferrocenyl naphthalene diimide can bind to DNA-RNA hetero duplex: Potential use in an electrochemical detection of mRNA expression, 2001; **637**: 476-483.
29. Murr MM, Harting MT, Guelev V, Ren JS, Chaires JB, Iverson BL. *Bioorg. Med. Chem.*, An octakis-intercalating molecule, 2001; **9**: 1141-1148.
30. Guelev V, Lee J, Ward J, Sorey S, Hoffman DW, Iverson BL. *Chem. Biol.*, Peptide bis-intercalator binds DNA via threading mode with sequence specific contacts in the major groove, 2001; **8**: 415-425.
31. Guelev V, Sorey S, Hoffman DW, Iverson BL. *J. Am. Chem. Soc.*, Changing DNA grooves - A 1,4,5,8-naphthalene tetracarboxylic diimide bis-intercalator with the linker (beta-ala)(3)-lys in the minor groove, 2002; **124**: 2864-2865.
32. Lee J, Guelev V, Sorey S, Hoffman DW, Iverson BL. *J. Am. Chem. Soc.*, NMR structural analysis of a modular threading tetra-intercalator bound to DNA, 2004; **126**: 14036-14042.
33. Chu YJ, Sorey S, Hoffman DW, Iverson BL. *J. Am. Chem. Soc.*, Structural characterization of a rigidified threading bisintercalator, 2007; **129**: 1304-1311.
34. Steullet V, Dixon DW. *Bioorg. Med. Chem. Lett.*, Design, synthesis and DNA-cleavage of Gly-Gly-His-naphthalene diimide conjugates, 1999; **9**: 2935-2940.

35. Dixon DW, Thornton NB, Steullet V, Netzel TL. *Inorg. Chem.*, Intramolecular electron transfer quenching of a photoexcited ruthenium(II) polypyridine naphthalene diimide intercalated in DNA scaffolding, 1999; **38**: 5526-5534.
36. Okamoto A, Nakamura T, Yoshida K, Nakatani K, Saito I. *Org. Lett.*, Site-selective DNA alkylation of GG steps by naphthalendiimide derivatives possessing enantiomeric epoxide, 2000; **2**: 3249-3251.
37. Tok JBH, Fenker J. *Bioorg. Med. Chem. Lett.*, Novel synthesis and RNA-binding properties of aminoglycoside dimers conjugated via a naphthalene diimide-based intercalator, 2001; **11**: 2987-2991.
38. Mokhir A, Zohm B, Fuessl A, Kraemer R. *Bioorg. Med. Chem. Lett.*, Synthesis and DNA binding properties of terminally modified peptide nucleic acids, 2003; **13**: 2489-2492.
39. Michel J, Bathany K, Schmitter JM, Monti JP, Moreau S. *Tetrahedron*, New ligand combinations for the efficient stabilization of short nucleic acid hairpins, 2002; **58**: 7975-7982.
40. Vicic DA, Odom DT, Nunez ME, Gianolio DA, McLaughlin LW, Barton JK. *J. Am. Chem. Soc.*, Oxidative repair of a thymine dimer in DNA from a distance by a covalently linked organic intercalator, 2000; **122**: 8603-8611.
41. Nunez ME, Noyes KT, Gianolio DA, McLaughlin LW, Barton JK. *Biochemistry*, Long-range guanine oxidation in DNA restriction fragments by a triplex-directed naphthalene diimide intercalator, 2000; **39**: 6190-6199.

42. Lewis FD, Letsinger RL, Wasielewski MR. *Acc. Chem. Res.*, Dynamics of photoinduced charge transfer and hole transport in synthetic DNA hairpins, 2001; **34**: 159-170.
43. Takada T, Kawai K, Fujitsuka M, Majima T. *Proc. Natl. Acad. Sci. USA*, Direct observation of hole transfer through double-helical DNA over 100 Å, 2004; **101**: 14002-14006.
44. Lewis FD, Wasielewski MR. *Top. Curr. Chem.*, Dynamics and equilibrium for single step hole transport processes in duplex DNA, 2004; **236**: 45-65.
45. Nakajima S, Akiyama K, Kawai K, Takada T, Ikoma T, Majima T, Tero-Kubota S. *Chemphyschem*, Spin-correlated radical pairs in synthetic hairpin DNA, 2007; **8**: 507-509.
46. Takenaka S, Yamashita K, Uto Y, Takagi M, Kondo H. *Denki Kagaku*, Electrochemistry of ferrocenyl naphthalene diimide derivative and its behavior on hairpin DNA immobilized electrode, 1998; **66**: 1329-1334.
47. Tansil NC, Xie H, Xie F, Gao ZQ. *Anal. Chem.*, Direct detection of DNA with an electrocatalytic threading intercalator, 2005; **77**: 126-134.
48. Komatsu M, Nojima T, Takenaka S. *Electrochemistry*, Analysis of electrochemical reaction of ferrocenylnaphthalene diimide captured by double-stranded DNA during the electrochemical detection of DNA hybridization, 2006; **74**: 65-67.

49. Steullet V, Dixon DW. *J. Chem. Soc. Perkin Trans. 2*, Stacking of bis(dicarboximides) as probed by ^1H NMR, 1999; 1547-1558.
50. Zhong CJ, Kwan WS, Miller LL. *Chem. Mater.*, Self-assembly of delocalized π -stacks in solution. Assessment of structural effects, 1992; **4**: 1423-1428.
51. Sissi C, Lucatello L, Krapcho AP, Maloney DJ, Boxer MB, Camarasa MV, Pezzoni G, Menta E, Palumbo M. *Bioorg. Med. Chem.*, Tri-, tetra- and heptacyclic perylene analogues as new potential antineoplastic agents based on DNA telomerase inhibition, 2007; **15**: 555-562.
52. Kheifets GM, Martyushina NV. *Zh. Org. Khim.*, Hydrolysis of *N,N'*-disubstituted diimides of 1,4,5,8-naphthalene tetracarboxylic acid. I. Structure of the hydrolysis products and equilibrium position in relation to pH of the medium, 1982; **18**: 1528-1535.
53. Kheifets GM, Martyushina NV. *Zh. Org. Khim.*, Hydrolysis of *N,N'*-disubstituted diimides of 1,4,5,8-naphthalene tetracarboxylic acid. II. Kinetics of reversible hydrolysis catalyzed by bases, 1982; **18**: 1537-1544.
54. Langhals H, Jaschke H, Bastani-Oskoui H, Speckbacher M. *Eur. J. Org. Chem.*, Perylene dyes with high resistance to alkali, 2005; 4313-4321.
55. Langhals H, von Unold P. *Angew. Chem. Int. Ed.*, Tetracarboxylic bisimide-lactam ring contraction - A novel type of rearrangement, 1995; **34**: 2234-2236.

56. Ponce P, Fomina L, Perez F, Fomine S. *J. Mol. Str. -Theochem*, Unusual behaviour of bis[omega-hydroxyalkyl]-1,8,4,5-naphthalenetetracarboxylic bisimides in bisimide-lactam ring contraction: Experimental and theoretical study, 2001; **541**: 131-139.
57. Barros TC, Cuccovia IM, Farah JPS, Masini JC, Chaimovich H, Politi MJ. *Org. Biomol. Chem.*, Mechanism of 1,4,5,8-naphthalene tetracarboxylic acid dianhydride hydrolysis and formation in aqueous solution, 2006; **4**: 71-82.
58. Ernst ML, Schmir GL. *J. Am. Chem. Soc.*, Isoimides. A kinetic study of reactions of nucleophiles with N-phenylphthalisoimide, 1966; **88**: 5001-5009.
59. Brochsztain S, Politi MJ. *Langmuir*, Solubilization of 1,4,5,8-naphthalenediimides and 1,8-naphthalimides through the formation of novel host-guest complexes with α -cyclodextrin, 1999; **15**: 4486-4494.
60. Takatani M, Yoshioka Y, Tasaka A, Terashita Z, Imura Y, Nishikawa K, Tsushima S. *J. Med. Chem.*, Platelet activating factor antagonists - Synthesis and structure activity studies of novel PAF analogs modified in the phosphorylcholine moiety, 1989; **32**: 56-64.
61. ElAhmad Y, Brion JD, Reynaud P, Averbeck D, Averbeck S. *Heterocycles*, Synthesis and photobiological activity of N-substituted 2-oxo-2H-1-benzopyran-3-(thio)carboxamides, 1996; **43**: 2169-2177.

62. Nagamatsu H, Okuyama T, Fueno T. *Bull. Chem. Soc. Jpn.*, Effects of boric acid on the rate and equilibrium of Schiff-base formation from salicylaldehyde, 1984; **57**: 2508-2514.
63. Rao G, Philipp M. *J. Org. Chem.*, Boronic Acid Catalyzed Hydrolyses of Salicylaldehyde Imines, 1991; **56**: 1505-1512.
64. Nagamatsu H, Okuyama T, Fueno T. *Bull. Chem. Soc. Jpn.*, Hydrolysis of N-salicylidene-2-methoxyethylamine - intramolecular general base catalysis and specific effects of boric acid, 1984; **57**: 2502-2507.
65. Yatsimirsky AK, Bezoudnova KY, Sakodinskaya IK. *Bioorg. Med. Chem. Lett.*, Boric Acid Effect on the Hydrolysis of 4-Nitrophenyl 2,3-Dihydroxybenzoate - Mimic of Borate Inhibition of Serine Proteases, 1993; **3**: 635-638.
66. Breemhaar W, Engberts JBFN. *J. Org. Chem.*, Stopped-Flow Study of Salt Effects on Hydroxide and Borate Ion Catalyzed-Hydrolysis of Covalent Para-Tolylsulfonylmethyl Perchlorate in Aqueous Borax Buffer Solutions, 1978; **43**: 3618-3621.
67. Camilleri P, Carey JV, Odell B, Williams DJ. *J. Chem. Soc. Perkin Trans. 2*, Combined Use of Kinetic and Crystallographic Data to Probe the Hydrolysis of A Simple Amide, 1988; 591-596.
68. D'Anna F, Liveri MLT, Noto R. *Arkivoc*, A kinetic study of the basic hydrolysis of 2-phenylethyl nitrite in the presence of borate buffer and beta-cyclodextrin, 2002; 187-197.

69. Perrin CL, Engler RE, Young DB. *J. Am. Chem. Soc.*, Bifunctional catalysis and apparent stereoelectronic control in hydrolysis of cyclic imidatonium ions, 2000; **122**: 4877-4881.
70. Noll BW, Jarboe CJ, Hass LF. *Biochemistry*, Kinetic Studies on Alkali-Catalyzed Hydrolysis and Epimerization of Model Alkyl and Hydroxyalkyl Dipeptides and Tripeptides, 1974; **13**: 5164-5169.
71. Brault D, Rougee M. *Biochem. Biophys. Res. Commun.*, Binding of Imidazole and 2-Methylimidazole by Hemes in Organic-Solvents - Evidence for 5-Coordination, 1974; **57**: 654-659.
72. Brochsztain S, Rodrigues MA, Politi MJ. *J. Photochem. Photobiol. A*, Inclusion complexes of naphthalimide derivatives with cyclodextrins, 1997; **107**: 195-200.
73. Eriksson SO, Meresaar U. *Acta Chem. Scand.*, Hydrolysis of anilides. 10. Kinetics and mechanisms for acid and alkaline hydrolysis of aminoacylanilides and ammonioacylanilide cations, 1971; **25**: 2697-2710.